Main Manuscript for

Transcranial direct current stimulation modulates primate brain dynamics across states of consciousness

Guylaine Hoffner[a,1,*], Pablo Castro[a,b,1], Lynn Uhrig[a,c], Camilo M. Signorelli[d,e,f], Morgan Dupont[a], Jordy Tasserie[g], Alain Destexhe[b], Rodrigo Cofre[b,h], Jacobo Sitt[i,2] and Bechir Jarraya[a,j,2,*].

[a]Cognitive Neuroimaging Unit, CEA, INSERM, Université Paris-Saclay, NeuroSpin Center, 91191 Gif-sur-Yvette, France
[b]Institute of Neuroscience (NeuroPSI), Paris-Saclay University, Centre National de la Recherche Scientifique (CNRS), 91191, Gif-sur-Yvette, France
[c]Department of Anesthesiology and Critical Care, Necker Hospital, AP-HP, Université de Paris Cité, 75015, Paris, France
[d]Department of Computer Science, University of Oxford, Oxford, 7 Parks Rd, Oxford OUX1 3QG
[e]Laboratory of Neurophysiology and Movement Biomechanics (LNMB), Université Libre de Bruxelles (ULB), Route de Lennik 808, CP 640, Building N, campus Erasme, 1070 Brussels
[f]Center for Philosophy of Artificial Intelligence, University of Copenhagen, Karen Blixens Plads 8, Copenhagen 2300, Denmark.
[g]Center for Brain Circuit Therapeutics, Department of Neurology, Brigham & Women's Hospital, Harvard Medical School, Boston, MA 02115, USA
[h] Centre Inria Université Côte d'Azur, Equipe Cronos, France
[i]Sorbonne Université, Institut du Cerveau - Paris Brain Institute - ICM, Inserm, CNRS, Paris 75013, France
[j]Department of Neurology, Hopital Foch, 92150, Suresnes, France

[1]Co-first authors
[2]Co-last authors

*To whom correspondence should be addressed. Emails: guylaine.hoffner@inserm.fr; bechir.jarraya@cea.fr.

Author Contributions: G.H., L.U., J.S., and B.J. designed research; G.H., L.U., M.D., J.T. and B.J. performed research; G.H., P.C., L.U., C.M.S., A.D., R.C., J.S., and B.J. analyzed data; B.J. secured funding; and G.H., P.C. and B.J. wrote the paper and all authors contributed to its editing.

Competing Interest Statement: The authors declare no competing interest.

Classification: Biological Sciences, Neuroscience.

Keywords: tDCS, fMRI, brain dynamics, consciousness, prefrontal cortex.

Abstract

The resting primate brain is traversed by spontaneous functional connectivity patterns that show striking differences between conscious and unconscious states. Transcranial direct current stimulation, a non-invasive neuromodulatory technique, can improve signs of consciousness in disorders of consciousness; however, can it influence both conscious and unconscious dynamic functional connectivity? We investigated the modulatory effect of prefrontal cortex (PFC) transcranial direct current stimulation (tDCS) on brain dynamics in awake and anesthetized non-human primates using functional MRI. In awake macaques receiving either anodal or cathodal tDCS, we found that cathodal stimulation robustly disrupted the repertoire of functional connectivity patterns, increased structure-function correlation, decreased Shannon entropy, and favored transitions towards anatomically-based patterns. Under deep sedation, anodal tDCS significantly altered brain pattern distribution and reduced structure-function correlation. The prefrontal stimulation also modified dynamic connectivity arrangements typically associated with consciousness and unconsciousness. Our findings offer compelling evidence that PFC tDCS induces striking modifications in the fMRI-based dynamic organization of the brain across different states of consciousness. This study contributes to an enhanced understanding of tDCS neuromodulation mechanisms and has important clinical implications for disorders of consciousness.

Main Text

Introduction

At rest, the spontaneous activity of the awake brain is highly structured. The brain dynamically transitions through various resting-state functional magnetic resonance imaging (rs-fMRI) patterns, which are thought to support specific cognitive functions (Deco, Jirsa, and McIntosh 2013; Fox et al., 2006; Vincent et al., 2006; Damoiseaux et al., 2006; Raichle et al., 2001; Calhoun et al., 2014; Preti, Bolton, and Van De Ville 2017; Baker et al., 2014; Deco, Jirsa, and McIntosh 2011). Interestingly, in non-human primates (NHPs), the induction of wakefulness and unconsciousness by different anesthetics is associated with strikingly different sequences and occurrences of transient brain patterns (Barttfeld et al., 2015; Uhrig et al., 2018). The conscious brain is traversed by a diverse and mobile set of functional brain patterns that deviate from anatomical connectivity. In contrast, the unconscious brain is characterized by transient functional patterns that are less diverse, stiffer, and more closely follow anatomical connectivity. Similar dynamic functional configurations are found in awake and sedated humans and generalize to other contexts of loss of consciousness, whether in patients with impaired consciousness or during sleep (Luppi et al., 2021; Huang et al., 2020; Demertzi et al., 2019; Golkowski et al., 2019; Castro et al., 2024). Ultimately, these different structure-function configurations are proposed as signatures of consciousness and unconsciousness, respectively.

Over the past twenty years, transcranial direct current stimulation (tDCS) has emerged as a popular non-invasive tool for clinicians and researchers to modulate brain activity (Narmashiri and

Akbari 2023; Lefaucheur et al., 2017). Two or more electrodes are attached to the subject's head, and a weak current is applied between them, producing an electric field, part of which crosses the skull and influences the activity of underlying neurons (Lefaucheur and Wendling 2019). In vivo and in vitro data suggest that tDCS acts through diverse, concurrent, and multiscale modes of action (Lefaucheur et al., 2017; Lefaucheur and Wendling 2019). Importantly, ongoing neural activity during tDCS administration is likely to be critical, as tDCS effects are state-dependent and primarily modulate active networks (Antal et al., 2007; Bikson, Name, and Rahman 2013; Li et al., 2019).

Recent studies suggest that tDCS may influence the level of consciousness. Anodal tDCS of the left dorsolateral prefrontal cortex (DLPFC) improves signs of consciousness in patients with disorders of consciousness (DOCs) (Thibaut et al., 2014; Angelakis et al., 2014; Hermann et al., 2020; Liu et al., 2023) and can increase rs-fMRI connectivity in some of these patients, both at the site of stimulation and in remote regions (Peng et al., 2022). However, the effects of PFC tDCS on resting-state dynamic brain patterns which are typically associated with consciousness have never been investigated. In healthy humans, tDCS can perturb both occurrences and transitions of some rs-fMRI co-activation patterns (CAPs) (using the DLPFC as a seed), suggesting that some elements of brain dynamics could be affected by tDCS in the awake resting brain. Anesthesia provides a unique model for studying consciousness, which, similarly to DOC, is characterized by the disruption or even the loss of consciousness (Luppi 2024). Additionally, anesthesia mechanisms involve several subcortical nuclei that are key components of the brain's sleep and arousal circuits (Kelz and Mashour 2019). The effects of tDCS on brain activity during anesthesia-induced loss of consciousness remain largely unexplored. Repeated stimulation of the rat motor cortex facilitates the return of the righting reflex and visual and working memory after isoflurane anesthesia (Mansouri and García 2021), suggesting that tDCS may represent a novel approach to accelerate recovery from general anesthesia (Kato and Solt 2021).

However, these studies left many questions unanswered. Does PFC tDCS possess the ability to remodel the functional and structural brain organization characteristic of the conscious and unconscious brain? For example, can it affect the order and relative frequency of fMRI brain connectivity patterns, as well as other aspects of brain dynamics, such as the structure-function correlation and the Shannon entropy (Demertzi et al., 2019)? If so, do the polarity (e.g., anodal versus cathodal), the intensity (e.g., 1 mA versus 2 mA), and the timing of the stimulation (e.g., during versus after the stimulation) perturb these metrics differently? Ultimately, does tDCS have enough perturbational power to affect the dynamic configurations of connectivity characteristic of consciousness and unconsciousness residing in cortical brain dynamics? Answering these questions may both advance our comprehension of the neural mechanisms underlying tDCS effects and provide meaningful information for clinicians.

This study aimed to determine whether tDCS targeting the PFC can modify the relationship between the structural and functional brain organization in fMRI signals in NHPs, either in the awake state or under deep propofol anesthesia. Our specific aims were to determine the effects of PFC tDCS on brain dynamics 1) in awake NHPs receiving either anodal or cathodal stimulation, 2) in deeply anesthetized NHPs receiving anodal stimulation at two different intensities, and 3) the time course of these putative changes relative to the stimulation (i.e., during and after the stimulation). Our results provide evidence that anodal prefrontal tDCS had only a marginal effect on brain dynamics in awake animals. In contrast, cathodal prefrontal tDCS significantly reorganized the functional repertoire in favor of anatomically similar brain patterns

without apparent behavioral modification. Moreover, both anodal and cathodal stimulation affected the Markov chain transitions between brain patterns, with some changes specific to ongoing stimulation and others to the post-stimulation period. Under anesthesia, anodal prefrontal tDCS delivered at an intensity of 2 mA, but not 1 mA, significantly reduced the structure-function correlation but did not fully restore the broad and rich dynamic repertoire of functional patterns characteristic of wakefulness, nor did it induce signs of arousal in the animals. Altogether, these findings illustrate the ability of tDCS to modulate conscious and unconscious brain dynamics in a polarity- and intensity-dependent manner.

Results

We established an experimental procedure that allowed tDCS and fMRI data acquisition from macaque monkeys (*Macaca mulatta*) in two states of consciousness: awake and under general anesthesia (Figure 1). To characterize the functional and structural brain organization in fMRI signals and how they are affected by the stimulation, we calculated the dynamic functional connectivity between 82 cortical regions of interest (ROIs) based on the CoCoMac anatomical database. We used the Hilbert transform to estimate the phase of fMRI signals at each TR and computed the coordination between the continuous fMRI time series across all ROIs. We then applied the unsupervised K-means algorithm to cluster the phase-based coherence matrices. This allowed for the identification of recurrent patterns of brain connectivity. Finally, we sorted the brain patterns based on their degree of similarity to the CoCoMac anatomical matrix. We calculated the relative occurrence rates of the patterns, the structure-function correlation (SFC), and the Shannon entropy for each vigilance state, electrode arrangement, and stimulation condition. A graphical overview of the overall analysis is shown in Figure 2.

In Figures 3-6, we present the results for brain patterns (or *k* clusters) fixed to 6, as this number was determined to be the best choice for maximizing the inter-pattern correlation variance (IPCV) when considering awake and anesthesia datasets together (Figure 2 - figure supplement 1). Additionally, we verified that varying the number of brain patterns (or *k* clusters) in the K-means algorithm from 3 to 10 did not change the principal findings in the paper (Figure 2 - figure supplements 2-4). Boxplots displaying the main measurables (slope's coefficient and Shannon entropy) as a function of said *k*-number of clusters were also done (figure supplement 1 of Figures 3, 5, 6 & 7) to further demonstrate the consistency of our results, regardless of the choice of *k*.

Polarity-dependent effects of prefrontal tDCS on the cortical dynamic connectivity in awake macaques

To examine whether tDCS can perturb the repertoire of functional connectivity patterns characteristic of the awake state, we collected a total of 288 fMRI runs before, during, and after the application of tDCS at an intensity of 2 mA in two macaque monkeys using two different electrode setups (Figure 1A). Representative structural images showing electrode placements on the head of the two awake monkeys are shown in Figure 1 - figure supplement 1A). Supplementary File 1 displays the complete set of structural images, showing that the two electrodes were accurately placed over the prefrontal cortex and the occipital cortex in a reproducible manner across awake sessions.

We performed the dynamic connectivity analysis on data from all five awake experimental conditions: before tDCS, during tDCS using anodal or cathodal montages, and after anodal or cathodal tDCS (Figure 3). The resulting patterns exhibited a variety of complex configurations of interregional connectivity. These included long-range positive/negative coherences (patterns 1 and 3), mostly frontal positive and parieto-occipital negative coherences (patterns 2 and 4), and almost strictly positive medium or low interregional coherences (patterns 5 and 6) (Figure 3A). We then calculated the probability distribution of the occurrence of each pattern across the stimulation conditions (Figure 3C). Brain pattern 6, referred to as the 'anatomical pattern' due to its highest correlation with the CoCoMac connectome, showed the most numerous and strongest differences in visit frequency. The time spent in this pattern increased sharply during and following stimulation with the cathodal montage compared to before stimulation and to the corresponding conditions with the anodal montage. This later finding shows the specificity of the effects of the cathodal stimulation. The time spent in brain state 5 was markedly shorter in the cathodal post-stimulation condition compared to pre-stimulation. Cathodal stimulation also shortened the time spent in brain state 3 during stimulation compared to the corresponding condition with the anodal montage. In sharp contrast, the distribution of pattern occupancies during or following stimulation with the anodal montage did not exhibit much change compared to pre-stimulation. These polarity-specific effects of prefrontal tDCS were further illustrated by plotting the occurrence rate per condition (Figure 3D). These results suggest that the cathodal stimulation lowered the occurrence of patterns with high frontal coherence (patterns 1, 3, and 5), but promoted the visit of patterns with predominant parieto-occipital coherence (patterns 2 and 4) or very low coherence (pattern 6). All significant statistics are shown in Table 4A. It should be noted that these alterations of brain dynamics were not accompanied by any obvious behavioral changes in the monkeys, as they continued to show consistent and optimal eye fixation rates (Table 2).

Next, we computed the Shannon entropy from the normalized histograms of occurrences (Figure 3E, Table 4A). The Shannon entropy was considerably lower during and after cathodal stimulation compared to before stimulation and during cathodal stimulation compared to during anodal stimulation. In contrast, the Shannon entropy was not affected by stimulation with the anodal montage, further supporting the polarity-dependent nature of the effects. This result implies that cathodal, but not anodal stimulation limits the degree of surprise held in the distribution of pattern rates. A lower Shannon entropy was reported in many different studies investigating anesthesia-induced loss of consciousness in humans (Golkowski et al., 2019; Castro et al., 2024), in macaques (Barttfeld et al., 2015; Uhrig et al., 2018), under sleep-induced loss of consciousness in humans (Patel et al., 2020; Castro et al., 2024), and in patients suffering from disorders of consciousness (Demertzi et al., 2019). Moreover, recovery from general anesthesia in humans (Patel et al., 2020; Castro et al., 2024) and restoration of arousal and wakefulness in anesthetized macaques by deep brain stimulation of the central thalamus (Tasserie et al., 2022; Luppi et al., 2024) were both associated with recovery of a higher Shannon entropy value.

We then evaluated the relationship between the centroids' presence rate and the anatomical backbone in monkeys. We plotted the presence rates of all the centroids, for all macaques, as a function of their SFC. Considering the averages of occurrence rates over the different conditions, we computed one linear regression (per condition), to show the overall linear relationship between the time spent in the various brain states and their similarity to the anatomical

connectivity for each condition (Figure 3F). We then repeated such computation but for all subjects and all conditions (Figure 3G), and performed statistics on these distributions (shown in Table 4A*)*. The slope was substantially heightened during and after stimulation with the cathodal montage compared to before stimulation. In addition, during stimulation and post-stimulation, the cathodal montage was associated with a significantly higher slope coefficient compared to the anodal montage. Consistent with our previous observations, the stimulation with the anodal montage had a negligible influence on this metric compared to the pre-stimulation condition. These results were not affected by the choice of the number of *k* clusters (Figure 3 - figure supplement 1), and similar results were obtained when the full analysis was repeated for *k* = 4 (Figure 3 - figure supplement 2), as suggested by the IPVC (Figure 2 - figure supplement 1). Further investigation of the variances in inter-region phase coherences of brain patterns, presented in Figure 3 - figure supplement 3, revealed two main findings. First, all the patterns exhibited some degree of lateral symmetry. Second, except for the pattern with the highest SFC, most patterns displayed high heterogeneity in their coherence variances and striking inter-pattern differences. These observations reflect both the segmentation of distinct functional networks across patterns and a topological organization within the patterns themselves: some regions showed a broader spectrum of synchrony with the rest of the brain, while others exhibited narrower distributions of coherence variances. For instance, unlike other brain patterns, pattern 5 was characterized by a high coherence variance in the frontal premotor areas and low variance in the occipital cortex, whereas pattern 3 had a high variance in the frontal and orbitofrontal regions. In addition, we performed the main analyses separately for the two monkeys, explored the inter-condition variability (Supplementary File 2), and computed classical measures of functional connectivity such as average FC matrices and functional graph properties (modularity, efficiency and density) of the visited FC states (Supplementary File 3). The separate analyses showed that the changes in slope and Shannon entropy were substantially more pronounced in one of the two monkeys, corroborating some of the effects captured in the ANOVA tests. In contrast, classical FC metrics did not show significant differences across stimulation conditions, highlighting the value of dynamic FC metrics to capture the neuromodulatory effects of tDCS.

Next, we analyzed the succession of brain states through the prism of a Markov chain. Both anodal and cathodal stimulations produced significant changes in probability transitions (Figure 4). The corresponding statistics are shown in Table 4B. Strikingly, cathodal stimulation induced much greater transition probabilities from brain states 1 and 2 to brain state 6 (Figure 4A). Conversely, transitions from brain states 2 to 3, from 5 to 2, and 6 to 5 were significantly reduced by cathodal stimulation. Other changes were observed only after cathodal stimulation, including an increase in the probability of transitioning from brain states 5 to 6 and a probability decrease of transitioning from states 6 to 3. Ultimately, cathodal PFC tDCS strongly promoted transitions to brain state 6 and weakly inhibited some transitions leaving this state. As for anodal stimulation, it significantly favored the transitions from brain states 3 to 5 and from 2 to 3, and reduced the transitions from brain states 2 to 4 and 1 to 5 (Figure 4B). While these effects weren't sustained post-stimulation, the transition from brain states 2 to 6 was significantly perturbed post-stimulation. Overall, anodal PFC tDCS weakly altered only a few transitions. Our results also show that the Markov chain transition probabilities are affected differently during and after tDCS. Some changes were observed only during ongoing current delivery, while others were specific to the post-stimulation condition. Importantly, the fact that both categories of changes were found in cathodal and anodal experiments suggests a general phenomenon.

Contrasting the effects of prefrontal tDCS on the dynamic connectivity patterns in wakeful macaques to unconscious dynamics

Dynamic connectivity configurations associated with consciousness have previously been identified by analyzing data from conscious and unconscious states together (Barttfeld et al., 2015; Uhrig et al., 2018; Demertzi et al., 2019; Castro et al., 2024). We therefore repeated our analysis of the data from all five awake experimental conditions pooled with the anesthesia pre-stimulation condition (Figure 5). All significant statistics are shown in Table 4C.

The six resulting brain patterns showed somewhat different trends in connectivity arrangements compared to the patterns that emerged from the analysis of the awake data alone. While patterns 1 and 2 closely matched the previously obtained awake patterns 1 and 2, the others showed distinct connectivity configurations (Figure 5A). As expected, both the awake and the anesthesia pre-stimulation conditions exhibited significant differences in the rates at which the six brain patterns occurred (Figure 5C,D). Pattern 1 was present in the awake pre-stimulation condition but virtually absent in the anesthesia pre-stimulation condition, whereas patterns 5 and 6 were predominant under anesthesia. These findings are consistent with previous dynamic rs-fMRI studies in macaques and humans (Barttfeld et al., 2015; Uhrig et al., 2018; Demertzi et al., 2019). The cathodal montage again produced strong perturbation effects. Compared to pre-stimulation, pattern 4, characterized by short-range frontal coherences, occurred for a significantly shorter time during and after stimulation. Pattern 6, the so-called anatomical pattern, showed differences between conditions, consistent with our previous analysis of the awake conditions. As previously observed, cathodal tDCS increased the occurrence rate of pattern 6, while anodal stimulation had no effect. Therefore, consistent with the prior analysis of the data taken from the awake conditions alone, the cathodal stimulation reduced the incidence of the pattern with a predominant frontal coherence (here, pattern 4), while it increased the incidence of the 'anatomical' pattern (pattern 6).

The Shannon entropy was found to be much lower in anesthetized monkeys than in awake animals (Figure 5E). This finding is consistent with previous studies in humans, regardless of whether unconsciousness was due to disorders of consciousness, deep sleep, or anesthesia (Demertzi et al., 2019; Castro et al., 2024). While anodal stimulation had no effect, prefrontal cathodal stimulation significantly diminished Shannon entropy, similar to the previous analysis (Figure 3E). Consistent with our previous results, the cathodal tDCS induced a direct and lasting effect that was captured in our SFC-frequency analysis, where the states with high SFC were more present compared to those with low SFC (Figure 5F,G). These perturbations were noticeable when considering each macaque, and the effects observed during and post-cathodal stimulation were strong enough to alter the slopes. Compared to pre-stimulation, the changes observed during and post-stimulation were significant and had a similar tendency: an increase in the SFC-slope's coefficient. Finally, these differences were specific to the cathodal montage, and the comparison between the two types of electrode arrangements again revealed statistically significant differences. These results remained robust regardless of the number of *k* clusters (Figure 5 - figure supplement 1). The variance in inter-regional phase coherence across brain patterns showed notably that pattern 4, in contrast to most other patterns, was characterized by a high variance in frontal premotor areas and a low variance in the occipital cortex (Figure 5 - figure supplement 2).

Effects of prefrontal tDCS on the dynamic connectivity patterns in anesthetized macaques

Due to the challenging nature of the experimental procedures under anesthesia, we limited the investigations to only one stimulation modality. We chose to deliver anodal stimulation to provide new information on the effects of tDCS under anesthesia as a model for disorders of consciousness and to increase the cortical excitability of the PFC in an attempt to wake up the sedated monkeys. We also adopted a slightly different experimental design, as we aimed to determine the effects of anodal tDCS of the PFC with increasing intensity. We acquired fMRI data before, during, and after tDCS delivered at an intensity of 1 mA, followed by a second block of stimulation at 2 mA (Figure 1B). Representative structural images showing electrode placements on the head of the two anesthetized monkeys are shown in Figure 1 - figure supplement 1B. The complete set of structural images can be found in Supplementary File 1. A total of 136 runs were acquired in two macaque monkeys. We also continuously monitored vital parameters related to hemodynamics, ventilation, and temperature (Table 3). The dynamic signal coordination analysis was applied to the collected data. All significant statistics are shown in Table 4D.

Compared to the patterns observed from the analysis of the awake conditions alone (Figure 3A), the patterns generated from this experimental setup showed different organizations of interconnectivity between regions, with patterns 2, 3, 4, and 5 displaying primarily frontal/prefrontal coherences (Figure 6A). Interestingly, in the 2 mA post-stimulation condition, brain states 2 and 5 presented an increase in their presence rates compared to pre-stimulation, while brain state 6 showed a decrease (Figure 6C). Plotting the frequency of pattern visits across conditions further illustrated the notable reduction in the prevalence of brain state 6, the higher occurrence rate of brain states 2 and 5, as well as a tendency for the effects of the stimulation to gradually rise as a function of stimulation intensity (Figure 6D). Comparisons of Shannon entropy were non-significant (Figure 6E). However, for the 2 mA post-stimulation condition, the slope coefficient was statistically reduced compared to pre-stimulation (Figure 6F,G). These results remained robust regardless of the number of *k* clusters (Figure 6 - figure supplement 1). While several human studies have reported that 1 mA transcranial stimulation induces aftereffects (e.g., (Jamil et al., 2017, 2020; Monte-Silva et al., 2010), the differences between the 1 mA post-stimulation and baseline conditions were not significant in our analyses. However, it is still possible that the 1 mA stimulation produced some effects below the threshold of significance that may contribute to the changes observed during and after the 2 mA stimulation.

Because the IPVC suggested that 9 brain patterns would be optimal to reach the maximum IPVC for the anesthesia dataset (Figure 2 - supplement 1), we repeated the complete analysis for *k*=9 (Figure 6 - figure supplement 2). Using *k*=9, we found even more perturbations in brain dynamics by tDCS than with *k*=6. Firstly, the 'anatomical' brain state's occurrence rate was significantly lower both during and following 2 mA stimulation. Additionally, brain states 5 and 8 (which resemble brain states 2 and 5 in the analysis with *k*=6 in Figure 6A) showed an increase in their occurrence during and following stimulation at 2 mA. Finally, the slope coefficient was significantly decreased during and after 2 mA stimulation compared to before. No effect on the Shannon entropy was observed. The variance in inter-region phase coherences of the brain patterns is displayed in Figure 6 - figure supplement 3 and showed a striking heterogeneity between the patterns. For example, pattern 5 had a low overall variance (except in the frontal cortex), while pattern 1 was the only pattern with a high variance in the occipital cortex. Analyses of the two monkeys separately showed that the changes in slope and Shannon entropy were bigger in one of the two monkeys but went in the same direction (Supplementary File 2), while classical FC

metrics still did not noticeable capture any changes or statistical differences between the different stimulation conditions (Supplementary File 4).

Next, we contrasted the data from all anesthesia conditions with the awake pre-stimulation condition, keeping k=6 for the k-means clustering (Figure 7). As expected, all the patterns except pattern 5 showed significantly different occurrence rates between the awake and anesthesia pre-stimulation conditions (Figure 7C), consistent with the previous contrasted analysis (Figure 5C) and the literature (Barttfeld et al., 2015; Uhrig et al., 2018; Demertzi et al., 2019). Compared to pre-stimulation, brain state 3, a high positive frontal coherence pattern, was visited more often, and brain state 6 less frequently in the 2 mA post-stimulation condition. The slope coefficient was statistically reduced compared to pre-stimulation (Figure 7G), regardless of the number of *k* clusters (Figure 7 - figure supplement 1). These results show that 2 mA anodal PFC stimulation can reconfigure unconscious brain dynamics under anesthesia, albeit it could not restore the full range of characteristics of awake cortical dynamics, such as the visit of brain pattern 1. In line with these findings, these modulations were not accompanied by any behavioral signs of awakening in the animals. Nevertheless, the stimulation did influence some vital parameters (heart rate, systolic and diastolic blood pressure) (Table 3), as previously reported (Gu et al., 2022; Rodrigues et al., 2022). The variance in inter-region phase coherences of brain patterns is displayed in Figure 6 - figure supplement 2.

Lastly, we studied how the Markov chain transitions between brain states across stimulation conditions under anesthesia. However, during and following stimulation, at both 1 and 2 mA, not a single transition passed the bootstrapping method, even when the confidence level was reduced to 90%. Thus, we could not interpret any possible changes in transition probability since those empirical transitions can't be considered specific nor temporally independent. As such, we do not show this analysis.

Discussion

The dynamic nature of brain activity and connectivity in resting-state fMRI has attracted considerable interest over the past years. In this study, we demonstrate that tDCS perturbs dynamic brain patterns in both awake and deeply sedated macaques. We also demonstrate that the dynamic cortical connectivity arrangements previously described as typifying consciousness and unconsciousness can be non-invasively influenced by the application of a low-intensity direct current via transcranial stimulation. Our findings are consistent with the hypothesis that tDCS directly affects brain dynamics. In the following, we discuss the implications and potential mechanisms associated with the dynamic changes induced by tDCS.

Cathodal prefrontal tDCS strongly perturbed cortical brain dynamics in awake macaques

In awake animals, our analysis showed that cathodal stimulation of the PFC markedly alters the relative prevalence of cortical signal coordination patterns (Figures 3 and 5). We found that the 'anatomical' pattern (pattern 6) was the most sensitive to cathodal stimulation. Our observations that the prevalence of this pattern and the transitions towards it are greatly enhanced by cathodal stimulation in a conscious wakeful context are both unexpected and surprising. One explanation might be that this pattern is related to transient drops in vigilance levels and that cathodal

stimulation might enhance such a phenomenon. Contamination of fMRI data by transient periods of microsleep has been shown to occur frequently in awake resting-state experiments (Tagliazucchi and Laufs 2014). Previous work suggested that tDCS over prefrontal or frontal regions can influence arousal, sleepiness, or sleep quality (Frase et al., 2016; Annarumma et al., 2018). For instance, cathodal bi-frontal tDCS delivered immediately before sleep has been found to increase total sleep time and decrease cortical arousal in healthy volunteers (Frase et al., 2016). However, in our experiments, the stimulated animals showed no tendency to drowsiness or any sudden restlessness in an attempt to resist sleep. Furthermore, the animals were not resting but engaged in a fixation task throughout the fMRI data acquisition. It is also worth noting that they achieved a similar success rate in the cathodal stimulation condition compared to the pre-stimulation and anodal stimulation conditions (Table 2). Therefore, our observations do not appear to be consistent with an increase in drowsiness or a reduction in vigilance resulting from cathodal stimulation.

Alternatively, other types of mental processes might be enhanced by cathodal tDCS, such as the tendency to mind-wander, to experience mind-blanking, or to enter a hypnotic state. A seminal study demonstrated that anodal prefrontal cortex stimulation can significantly enhance the tendency to mind wander in healthy adults (Axelrod et al., 2015). However, subsequent efforts to replicate these findings yielded conflicting results (Coulborn and Fernández-Espejo 2022; Nawani, Mittner, and Csifcsák 2023). Mind-blanking is a state where the mind is alert but not actively engaged in a specific cognitive task. Reports of mind-blanking were recently found to correlate with a pattern of global positive-phase coherence rather than the pattern that most closely resembles anatomy (Mortaheb et al., 2022). This finding does not support an enhancement of mind-blanking by cathodal stimulation of the PFC in our study.

Finally, cathodal left DLPFC tDCS was demonstrated to enhance hypnotizability by 15% and to alter some dimensions of consciousness, significantly increasing attention, absorption, and time sense but decreasing self-awareness and memory (Perri et al., 2022; Perri and Di Filippo 2023). While our observations of the monkey's high fixation task performance would be consistent with increased attention or absorption, the demonstration of a modulatory effect of cathodal tDCS on one or other of these specific mental processes or dimensions of consciousness will require further investigation in humans using relevant behavioral measures, cognitive tasks, and brain activity tracking.

Anodal prefrontal tDCS perturbed cortical brain dynamics, especially during deep anesthesia

In awake macaques, we found that the anodal montage significantly disturbed some transition probabilities between brain states (Figure 4C,D). Anodal stimulation tended to decrease the slope's coefficient (Figures 3G and 5G) and to increase the occurrence rate of brain state 1 (Figures 3C,D and 5C,D). Although small, these changes are consistent with recent literature suggesting that anodal PFC tDCS, when delivered during the daytime, can positively influence levels of vigilance and sleepiness (Annarumma et al., 2018). For example, this type of stimulation has been described to increase beta and decrease delta powers in a wakeful context, thus indicating enhanced vigilance (Wirth et al., 2011; Maeoka et al., 2012; Dai et al., 2022). Bifrontal anodal stimulation increased both objective and subjective vigilance, and reduced daytime sleepiness in a patient with organic hyperinsomnia following reanimation (Frase et al., 2015). Moreover, in sleep-deprived adults, bifrontal anodal tDCS also reduced EEG correlates of

physiological sleepiness (Alfonsi et al., 2023). Anodal left DLPFC tDCS performed better than caffeine in preventing the reduction in vigilance and alleviating subjective ratings of fatigue and drowsiness in sleep-deprived individuals (McIntire et al., 2014). Finally, such a stimulation affected total sleep time, shortening it by about 25 min, when administered just before sleep in healthy volunteers (Frase et al., 2016).

While we observed modest effects of anodal PFC tDCS in awake animals, the stimulation produced significant changes in cortical brain dynamics under anesthesia and reduced the structure-function correlation, suggesting a state in-between wakefulness and anesthesia (Figures 6 and 7). Therefore, although our protocol did not succeed in awakening the sedated animals, our results support the ability of prefrontal tDCS to affect brain dynamic patterns related to consciousness in the context of an anesthesia-induced loss of consciousness. We hypothesize that the molecular effect of the anesthetic drug was stronger than the electrical effect at an intensity of 2 mA, which could explain the lack of behavioral effects. However, a similar protocol could succeed in awakening macaques sedated with a lower dose of propofol or in reversing unconsciousness due to deep propofol anesthesia with a higher stimulation intensity. In this case, the effects may reach a threshold where we get as much disturbance from pharmacology as physical intervention, thus resulting in an observable behavioral effect of tDCS. This idea is supported by the fact that we observed a greater effect on brain dynamics at 2 mA compared to 1 mA. Interestingly, a recent study in humans showed that tDCS delivered at 4 mA intensity can robustly enhance the effects of stimulation compared to 2 mA and is safe, well-tolerated, and without adverse effects (Nitsche and Bikson 2017; Hsu et al., 2023). Therefore, our results encourage further investigation using anodal prefrontal tDCS at an intensity of 4 mA to non-invasively attempt to reverse the effects of deep propofol anesthesia. Our findings also support the use of tDCS to promote rapid recovery from general anesthesia in humans (Kato and Solt 2021) and suggest that a single anodal prefrontal stimulation at the end of the anesthesia protocol may be effective.

From another clinical perspective, our results demonstrating that 2 mA anodal PFC tDCS decreased the structure-function correlation and modified the dynamic repertoire of brain patterns during anesthesia (Figures 6 and 7) are consistent with the beneficial effects of such stimulation in DOC patients (Thibaut et al., 2014; Angelakis et al., 2014; Thibaut et al., 2017; Zhang et al., 2017; Martens et al., 2018; Cavinato et al., 2019; Wu et al., 2019; Hermann et al., 2020; Peng et al., 2022; Thibaut et al., 2023). Although some clinical trials investigated the effects of stimulating other brain regions, such as the motor cortex (Martens et al., 2019; Straudi et al., 2019) or the parietal cortex (Huang et al., 2017; Guo et al., 2019; Zhang et al., 2022; Wan et al., 2023; Wang et al., 2020), the DLPFC appears to be the most effective target for patients with a minimally conscious state (Liu et al., 2023). In terms of neuromodulatory effects in DOC patients, DLPFC tDCS has been reported to increase global excitability (Bai et al., 2017), increase the P300 amplitude (Zhang et al., 2017; Hermann et al., 2020), improve the fronto-parietal coherence in the theta band (Bai et al., 2018), enhance the putative EEG markers of consciousness (Bai et al., 2018; Hermann et al., 2020) and reduce the incidence of slow-waves in the resting state (Mensen et al., 2020). Our findings further support the PFC as a relevant target for modulating consciousness level and align with growing evidence showing that the PFC plays a key role in conscious access networks (Mashour, Pal, and Brown 2022; Panagiotaropoulos 2024). Nevertheless, we hypothesize that other brain targets for tDCS may be of interest for consciousness restoration, potentially using multi-channel tDCS (Havlík et al., 2023). Among transcranial electrical stimulation techniques, tDCS has the great advantage of facilitating either

excitation or inhibition of brain regions, depending on the polarity of the stimulation (Sdoia et al., 2019) exploited this advantage to investigate the causal involvement of the DLPFC in conscious access to a visual stimulus during an attentional blink paradigm. While conscious access was enhanced by anodal stimulation of the left DLPFC compared to sham stimulation, opposite effects were found with cathodal stimulation compared to sham over the same locus. Finally, this literature and our findings suggest that tDCS constitutes a non-invasive, reversible, and powerful tool for studying consciousness.

Changes in the state of consciousness are generally closely associated with changes in behavioural responsiveness, although some rare cases of dissociation have been described. Cognitive-motor dissociation (CMD) is a condition observed in patients with severe brain injury, characterized by behavior consistent with unresponsive wakefulness syndrome or a minimally conscious state minus (Thibaut et al., 2019). However, in these patients, specific cortical brain areas activate in response to mental imagery tasks (e.g., imagining playing tennis or returning home) in a manner indistinguishable from that of healthy controls, as shown through fMRI or EEG (Thibaut et al., 2019; Owen et al., 2006; Monti et al., 2010; Bodien et al., 2024). Thus, although CMD patients are behaviorally unresponsive, they demonstrate cognitive awareness that is not outwardly apparent. It is worth noting that both the structure-function correlation and the rate of the pattern closest to the anatomy were shown to be significantly reduced in unresponsive patients showing command following during mental imagery tasks compared to those who do not show command following (Demertzi et al., 2019). These observations would be compatible with our findings in anesthetized macaques exposed to 2 mA anodal PFC tDCS. The richness of the brain dynamics would be recovered (at least partially, in our experiments), but not the behaviour. This hypothesis also fits with a recent longitudinal fMRI study on patients recovering from coma (Crone et al., 2020). The researchers examined two groups of patients: one group consisted of individuals who were unconscious at the acute scanning session but regained consciousness and improved behavioral responsiveness a few months later, and the second group consisted of patients who were already conscious from the start and only improved behavioral responsiveness at follow-up. By comparing these two groups, the authors could distinguish between the recovery of consciousness and the recovery of behavioral responsiveness. They demonstrated that only initially conscious patients exhibited rich brain dynamics at baseline. In contrast, patients who were unconscious in the acute phase and later regained consciousness had poor baseline dynamics, which became more complex at follow-up. Complete recovery of both consciousness and responsiveness under general anesthesia is possible through electrical stimulation of the central thalamus (Redinbaugh et al., 2020; Tasserie et al., 2022).

From a mechanistic point of view, prefrontal tDCS may modulate arousal and improve the level of consciousness by acting on the recently proposed cortico-thalamic pathway of sleep-wake regulation or by acting directly on the ascending thalamocortical pathway, which originates in the brainstem (Krone et al., 2017). Depending on electrode positions and stimulation parameters, tDCS has been shown to modulate subcortical regions directly. For example, fronto-temporal tDCS has been reported to alter corticostriatal and corticothalamic rs-fMRI connectivity in healthy volunteers (Polanía, Paulus, and Nitsche 2012; Dalong et al., 2020). In vivo measurements in humans using intracerebral electrodes confirmed that the stimulation can generate a biologically relevant electric field at the subthalamic level or other deep brain structures (Guidetti et al., 2022; Louviot et al., 2022). Computational modelling of the electric field (Saturnino et al., 2019; Huang et al., 2012) generated by the specific fronto-occipital montage used in this study will likely yield valuable information regarding which pathway (cortico-thalamic or thalamocortical) may have

been modulated. Furthermore, modulation of intrinsic networks (Raichle et al., 2001; Boly et al., 2008) is possible in light of our result and could also be investigated through an iCAPs-based analysis (Karahanoğlu and Van De Ville 2015; Ensel et al., 2023).

From a biophysical standpoint, previous studies showed that anodal stimulation leads to depolarization at the soma of neurons in rat hippocampal slices, while cathodal stimulation induces their hyperpolarization, especially when the current is aligned with the soma-apical axis (Bikson et al., 2004). These findings were corroborated in human subjects (Nitsche and Paulus 2000), where anodal tDCS applied to the motor cortex increased the amplitude of motor-evoked potentials in response to transcranial magnetic stimulation, while cathodal M1 stimulation had the opposite effects, revealing an increase or decrease in M1 excitability, respectively. The magnitude of these effects was small (0.2 mV) (Bikson et al., 2004) but fell within the range of endogenous electric field interactions generated between cortical columns, where it can be greatly amplified by recurrent interactions (Rebollo et al., 2021). Interestingly, in the awake state, we observed that cathodal stimulation of the PFC induced a significant decrease in the frequencies of patterns exhibiting high frontal coherence (patterns 3 and 5), which is consistent with a reduction in PFC excitability under the cathodal electrode. In contrast, the stimulation with this montage tended to increase the frequency of patterns with a predominant parieto-occipital coherence (patterns 2 and 4), which is in line with an increase in excitability under the anodal electrode positioned over the occipital cortex (Figure 3A,C). Under anesthesia, 2 mA anodal tDCS of the PFC increased the frequencies of some patterns exhibiting a high frontal coherence (patterns 2 and 5) (Figure 6A,C), also supporting enhanced excitability under the anodal electrode in deep sedation. It is important to note that the effects of the neuromodulatory ascending systems on brain activation are known to be mediated both by neuronal depolarization and by inhibition of voltage and calcium-dependent conductance, which are responsible for spike-frequency adaptation in pyramidal cells (Steriade and McCarley 2013; McCormick 1992). Therefore, one possible explanation for the inability of anodal stimulation of the PFC to arouse macaques from anesthesia is that it caused depolarization of neurons without affecting spike-frequency adaptation and thus only partially activated the brain.

Markov chain analysis revealed differential tDCS effects on transition probabilities during and after stimulation

Our results showed relatively similar effects during and after the stimulation in terms of brain pattern occurrence rates, Shannon entropy, and SFC (Figures 3, 5, 6, 7). In contrast, Markov chain analysis revealed the existence of specific changes in transition probability induced by tDCS, some of which were found only during stimulation and others exclusively in the post-stimulation condition (Figure 4, Table 4B). Our results highlight that certain effects of tDCS on brain dynamics are specific to the time course of the stimulation and can be revealed using particular dynamic analyses such as the Markov chain transition.

In conclusion, our data provides experimental evidence that tDCS of the prefrontal cortex modulates spontaneous brain activity whether the animals are wakeful and conscious, or unconscious under general anesthesia. Our study offers a deeper understanding of how tDCS influences and alters brain dynamics, which is crucial given its growing applications in neuroscience and the management of various neurological conditions. Finally, our work suggests that by allowing a soft, non-invasive and reversible perturbation of brain activity, tDCS may be a

valuable tool for further investigations of the relationship between brain dynamics and states of consciousness, conscious processing, or vigilance.

Materials and Methods

Animals

Four rhesus monkeys (*Macaca mulatta*, 18-20 years, 7.2-9.8 kg) were scanned. Two males were tested for the awake experiments (monkeys J and Y), and one female and one male were tested for experiments under anesthesia (monkeys R and N). Our sample size is comparable to previous work in NHP using fMRI (Milham et al., 2018; Yacoub et al., 2020; Uchimura, Kumano, and Kitazawa 2024).
All procedures followed the European Convention for Animal Care (86-406) and the National Institutes of Health's Guide for the Care and Use of Laboratory Animals. Animal studies were approved by the Institutional Ethical Committee (CETEA protocol #16-040).

Transcranial Direct Current Stimulation

We applied tDCS using a battery-powered stimulator (1x1 tES device, Soterix medical) located outside the scanner room and a complete MR-compatible setup consisting of an MRI filter, carbon composition cables (Soterix medical). We used a 1x1 electrode montage with two carbon rubber electrodes (dimensions: 1.4 cm x 1.85 cm, 0.93 cm thick) inserted into Soterix HD-tES MRI electrode holders (base diameter: 25 mm; height: 10.5 mm), which are in contact with the scalp. These electrodes (2.59 cm^2) are smaller than conventional tDCS sponge electrodes (typically 25 to 35 cm^2). The electrode setups and experimental designs used in awake and anesthetized macaques are shown in Figure 1.

Electrode contact quality was checked before all stimulation sessions using the device's Pre-stim Tickle function (1 mA for 30 s). If a poor contact was detected, the electrode-scalp contact was readjusted, and conductive paste or gel was added to improve contact quality. Electrode contact quality was continuously monitored during the stimulation.

To reduce the likelihood of the monkeys experiencing discomfort at the electrode sites, the current was gradually increased from 0 mA to the target intensity over the first 30 seconds. The current was also gradually decreased to 0 mA over the last 30 seconds of each tDCS stimulation period. The tDCS device was turned off during the acquisition of the pre- and post-stimulation fMRI blocks to avoid any hypothetical biological effect of the residual current (Fonteneau et al., 2019), which we measured to be 0.023 mA. After the tDCS-fMRI scanning sessions, the monkeys' scalps were examined for redness, skin burns, or other lesions. None of the monkeys showed any side effects.

Awake experiments
In the awake experiments, elastic bands with fasteners were used to secure the electrode holders. We used a conductive and adhesive paste (Ten20 conductive paste, Weaver and Company) to ensure consistent electrode-skin contact. The anode electrode was placed over the left PFC (F3) and the cathode electrode over the right occipital cortex (O2), or the reverse montage was employed, with the cathodal electrode placed over the right PFC (F4) and the

anode over the left occipital cortex (O1) (Figure 1A). We used monkey EEG caps (EasyCap, 13 channels, Fp1, Fp2, F3, F4, T3, T4, P3, P4, O1, O2, Oz, reference electrode, ground electrode), based on the international 10-20 EEG system, to obtain F3, F4, O1, and O2 locations, where we placed the stimulation electrodes. The two montages were respectively abbreviated F4/O1 and O1/F4. tDCS was delivered for 20 min at a current intensity of 2 mA.

Anesthesia experiments

For anesthesia experiments, the electrode holders were held in place with Monkey-2D caps (EasyCaps GmbH), using an EEG gel to obtain low impedance (One Step EEG gel, Germany) as the conductive medium. Monkey R was stimulated with an F3/O2 montage (anodal electrode over the left PFC and cathodal electrode over the right occipital cortex) and monkey N was stimulated with an F4/O1 montage (anodal electrode over the right PFC and cathodal electrode over the left occipital cortex) (Figure 1B). This different but still close placement of the electrodes between the two animals was dictated by constraints related to the location of the headpost (with the cement used to anchor the headpost spreading more or less asymmetrically) and the anatomy/specificity of each animal's head. Because of the small size of the monkey's head and because we did not use return electrodes to restrict the current flow (as is achieved with typical high-definition montages (Datta et al., 2009; Alam et al., 2016)), we expected that tDCS stimulation with the two symmetrical montages would result in nearly equivalent electric fields across the monkey's head and produce roughly similar effects on brain activity. This would need to be confirmed by running an electric field simulation. However, computational electric field models have been developed for humans, and their use in NHPs is not straightforward due to anatomical specificities. Indeed, monkeys differ from humans in terms of brain size, shape and cortical organization, skull thickness, tissue conductivities and the presence of muscles (Lee et al., 2015; Datta et al., 2016; Mantell et al., 2023). Modelling of EFs generated with the specific tDCS montages employed in this study will be performed in future work. Two 20-minute blocks of anodal tDCS stimulation were applied consecutively in each scanning session, with a current intensity of 1 mA for the first block and 2 mA for the second block (Figure 1B).

<u>fMRI Data Acquisition</u>

The monkeys were scanned on a 3-T horizontal scanner (Siemens Prisma Fit, Erlanger, Germany) with a custom-built single transmit-receiver surface coil. The parameters of the fMRI sequences were as follows: (i) functional scan: EPI, TR = 2400 ms, TE = 20 ms, 1.5-mm isotropic voxel size, and 111 brain volumes per run, (ii) anatomical scan: MPRAGE, T1-weighted, TR = 2200 ms, TE = 3,18 ms, 0.80-mm isotropic voxel size, sagittal orientation. Before each scanning session, monocrystalline iron oxide nanoparticles (10 mg/kg, i.v.; MION, Feraheme, AMAG Pharmaceuticals, MA) were injected into the saphenous vein of the monkey to improve the contrast-to-noise ratio and the spatial selectivity of the MR signal changes (Vanduffel et al., 2001).

All fMRI data were acquired while the monkeys were engaged in a passive event-related auditory task, the local-global paradigm, which is based on local and global deviations from temporal regularities (Bekinschtein et al., 2009; Uhrig, Dehaene, and Jarraya 2014). The present paper does not address how tDCS perturbs cerebral responses to local and global deviants, which will be the subject of future work. fMRI data were acquired before tDCS stimulation, during tDCS stimulation (onset of fMRI acquisition starting after the ramp-up period and stopping before the ramp-down period), and after tDCS stimulation. For anesthesia experiments, a second round of

stimulation/post-stimulation block was completed (see below). Four runs of 111 brain volumes were acquired during each condition (before tDCS stimulation, during tDCS stimulation, and after tDCS stimulation). Finally, all sessions ended up with an anatomical scan.

Awake protocol

Monkeys were implanted with an MR-compatible headpost, trained to sit in a sphinx position in a primate chair, and to fixate within a 2×2° window centred on a red dot (0.35×0.35°) within a "mock" MR bore before being scanned. fMRI data were acquired in awake macaques as previously described (Uhrig, Dehaene, and Jarraya 2014). The eye position was monitored at 120 Hz (Iscan Inc., MA, USA) and the fixation rate during the fMRI run was recorded (Table 2). To ensure that the results were not biased by fatigue or drowsiness due to the lengthy experimental procedure, only runs with a fixation rate > 85% were included in the analysis. No physiological parameters were recorded in the awake state.

A total of 288 runs were acquired in the awake state: 136 runs before stimulation, 56 runs during anodal stimulation, 56 runs after anodal stimulation, 20 runs during cathodal stimulation, and 20 runs after cathodal stimulation (see Table 1 for details of the number of runs acquired per monkey).

Anesthesia protocol

The anesthesia protocol is described in detail in a previous study (Tasserie et al., 2022). Anesthesia was induced with an intramuscular injection of ketamine (10mg/kg, Virbac, France) and dexmedetomidine (20 µg/kg, Ovion Pharma, USA) and maintained with a target-controlled infusion (TCI) (Alaris PK Syringe pump, CareFusion, CA, USA) of propofol (Panpharma Fresenius Kabi, France) using the "Paedfusor" pharmacokinetic model (Absalom and Kenny, 2005;) (Monkey R: TCI 5.8 µg/mL, Monkey N: TCI 4.3 µg/mL). Monkeys were intubated and mechanically ventilated. The physiological parameters (heart rate, noninvasive blood pressure, oxygen saturation, respiratory rate, end-tidal carbon dioxide, and skin temperature) were monitored (Maglife, Schiller, France) and recorded (Table 3). A muscle-blocking agent (cisatracurium, GlaxoSmithKline, France, 0.15 mg/kg, bolus i.v., followed by a continuous infusion rate of 0.18mg/kg/h) was used during all anesthesia fMRI sessions to avoid artifacts.

We referred to a clinical arousal scale at the beginning and end of each scanning session to characterize the behavior of monkeys in experiments under anesthesia. This scale comprises several indicators: an exploration of the environment, spontaneous movements, shaking/prodding, toe pinch, eye-opening, and corneal reflex (for more details, see (Uhrig et al., 2016; Tasserie et al., 2022).

A total of 136 runs were acquired under anesthesia: 40 runs before stimulation, 24 runs during 1 mA anodal stimulation, 24 runs after 1 mA anodal stimulation, 24 runs during 2 mA anodal stimulation, and 24 runs after 2 mA anodal stimulation (see Table 1 for details of the number of runs acquired per monkey).

<u>Statistical Analysis of the Physiological Data</u>

One-way analysis of variance (ANOVA) was used to compare the effect of the stimulation on mean heart rate, blood pressure, and other vital parameters under anesthesia (Table 3).

Statistical analysis and multiple comparisons were performed using home-made MATLAB scripts (MathWorks, USA), with a statistical threshold of $p < 0.05$, Bonferroni-corrected.

fMRI Data Analyses

fMRI preprocessing

Functional images were reoriented, realigned, resampled (1 mm isotropic), smoothed (Gaussian kernel, 3 mm full width at half maximum), and rigidly co-registered to the anatomical template of the monkey MNI space (Frey et al., 2011) using custom-made scripts (Uhrig, Dehaene, and Jarraya 2014).

The global signal was regressed out from the images to remove any confounding effects due to physiological changes (e.g., respiratory or cardiac variations). Voxel time series were filtered with low-pass (0.05 Hz cutoff) and high-pass (0.0025 Hz cutoff) filters and a zero-phase fast Fourier notch filter (0.03 Hz) to remove an artifactual pure frequency present in all the data (Barttfeld et al., 2015; Uhrig et al., 2018).

An additional cleaning step was performed to check the data quality after time series extraction, as described previously (Signorelli et al., 2021). The procedure was based on a trial-by-trial visual inspection by an expert in neuroimaging of the time series for all nodes, the Fourier transform of each signal, the functional connectivity for each subject, and the dynamical connectivity computed with phase correlation. For each dataset, visual inspection was first used to become familiar with the characteristics of the entire dataset: how the amplitude spectrum, time series, FC, and dynamic FC look. Subsequently, each trial was inspected again with a particular focus on two main types of potential artefacts. The first one corresponds to potential issues with the acquisition and is given by stereotyped sinusoidal oscillatory patterns without variation. The second one refers to potential head or other movement not fully corrected by our preprocessing procedure. This last artefact can be sometimes recognized by bursts or peaks of activity. Sinusoidal activity generates artificially high functional correlation and peak of frequencies in the amplitude spectrum plot. Uncorrected movements generate peaks of activity with high functional correlation and sections of high functional correlations in the dynamical FC matrix. If we observed any of these anomalies we rejected the trial, opting to adopt a conservative policy. Trials were retained if the row signal showed no evidence of artifactual activity, the functional connectivity was coherent with the average and the dynamical connectivity showed consistent patterns over time.

Finally, a total of 295 runs were analyzed in the following conditions: awake state, 190 runs (before tDCS, 82 runs; during anodal tDCS, 38 runs, after anodal tDCS, 39 runs, during cathodal tDCS, 15 runs, after cathodal tDCS, 16 runs) and anesthesia, 105 runs (before tDCS, 34 runs; during 1 mA anodal tDCS, 18 runs; after 1 mA anodal tDCS, 18 runs; during 2 mM anodal tDCS, 17 runs; after 2 mA anodal tDCS, 18 runs).

Anatomical Parcellation and Structural Connectivity

Anatomical connectivity data were obtained from a recent macaque connectome generated by coupling diffusion MRI tractography with axonal tract tracing studies (Bakker, Wachtler, and Diesmann 2012; Shen et al., 2019). The macaque cortex was subdivided using the Regional Map parcellation method (Kötter and Wanke 2005). The parcellation includes 82 cortical regions of

interest (41 ROIs per hemisphere). Structural (i.e., anatomical) connectivity data are represented as matrices in which the 82 cortical regions of interest are plotted on the x-axis and y-axis. The CoComac connectivity matrix contains information about the strength of the connections between cortical areas, with each cell representing the connection between any two regions.

Signals Representation

Given a real-valued signal $x(t)$, there exists a unique analytic representation $\tilde{x}(t)$, which is a complex signal, with the same Fourier transform as the real-valued signal strictly defined for positive frequencies. This analytic signal can be constructed from the real-valued signal using the Hilbert transform H:

$$\tilde{x}(t) = x(t) + iH[x(t)] \qquad (1)$$

i being the squared root of -1, the imaginary unit. The motivations for using the analytic signal are that, given some real-value data (i.e. MION signals), one can determine two functions of time that provide more meaningful properties of the signal. For a narrowband signal that can be written as an amplitude-modulated low-pass signal $A(t)$ with carrier frequency expressed by $\varphi(t)$:

$$x(t) = A(t)\cos[\varphi(t)] \qquad (2)$$

Then, if the Fourier transforms of $A(t)$ and $\cos[\varphi(t)]$ have separate supports, the analytic signal of a narrowband signal can be rewritten as the product of two meaningful components

$$\tilde{x}(t) = A(t)e^{i\varphi(t)} \qquad (3)$$

Where $A(t)$ is the instantaneous amplitude, $\varphi(t)$ the instantaneous phase obtained from the Hilbert transform $H[x(t)]$.

The narrower the bandwidth of the signal of interest, the better the Hilbert transform produces an analytic signal with a meaningful envelope and phase (Glerean et al., 2012). Adopting a band-pass filtered version of the MION time series $x(t)$ improves the separation between the phase and envelope spectra. The time series were z-scored, and subsequently, the Hilbert transform was computed to obtain the phase of each signal at each volume and each moment (TR, i.e. one-time sample).

Phase-based Dynamic Functional Coordination

A recurrent issue in fMRI studies dealing with dynamical analysis is the arbitrary choices in the time-windows length and their overlapping when capturing temporal oscillations through a sliding-window methodology (Hindriks et al., 2016; Xie et al., 2019; Allen et al., 2014; Barttfeld et al., 2015). Thus, phase-based dynamic functional coordination was preferred (Alonso Martínez et al., 2020; Cabral et al., 2017; Vohryzek et al., 2020; Demertzi et al., 2019). Analytic representations of signals were employed to derive a phase signal corresponding to the MION

time series. We computed the instantaneous phase $\varphi_n(t)$ of the signals across all regions of interest (ROI) $n \in \{1, ..., N\}$ for each repetition time (TR) $t \in \{2, \ldots, T-1\}$. The first and last repetition time (TR) of each fMRI scan were excluded due to possible signal distortions induced by the Hilbert transform (Bracewell 2000).

The instantaneous phase was computed using Euler's formula from the analytic signal, which was then "enfolded" within the range of $-\pi$ to π, facilitating the calculation of inter-ROI phase differences. To obtain a whole-brain pattern of phase differences, the phase coherence between pairs of areas k and j at each time t, labeled $PC(k, j, t)$, was estimated using the pairwise phase coherence defined as the cosinus of the angular difference:

$$PC(k, j, t) = \cos(\varphi_k(t) - \varphi_j(t)) \quad (4)$$

When areas k and j have synchronized MION signals at time t, the phase coherence takes the value 1, and when areas k and j are in anti-phase at time t, their associated phase coherence is -1. All the intermediate cases lie in between the interval $[-1, 1]$. This computation was repeated for all subjects. For each subject, the resulting phase coherence was a three-dimensional tensor with dimension $N \times N \times T$, where N is the total number of regions in the parcellation (here 82 regions) and T the total number of TR in each fMRI session. One can easily see the symmetry with respect to the spatial dimensions ($PC(k, j, t) = PC(j, k, t)$). Hence, only the triangular superior parts of the phase coherence matrices were used for later computations, thus reducing the phase space's size to $\frac{N \times (N-1)}{2}$ (the diagonal was omitted) and containing the useful available information.

K-Means Clustering

To assess recurring coordination patterns among individuals in both datasets, a multistep methodology was employed. First, the scanning sessions were transformed into matrices, wherein one dimension represented instantaneous phase differences (feature space), as explained above, and the other dimension represented time. We concatenate all the vectorized triangular superior parts for all subjects at all times and from the experimental conditions, hence obtaining phase-spaces over time matrices, one for each condition. Each resulting matrix was subjected to the k-means clustering algorithm utilizing the L2 "Euclidean" distance metric. This resulted in a discrete set of k coordination patterns and their corresponding occurrence over time.

This process yielded k cluster centroids, which served as representatives of the recurring coordination patterns, accompanied by a label indicating the closest pattern for each instantaneous phase difference at every given TR.

The number of clusters was determined for a range $k = \{3, ..., 10\}$, with 100 initializations and 200 iterations each, using the 'k-means++' initialization method, respectively to ensure a maximum (or minimum) value for metrics used as a proxy for choosing the optimal k-number of clusters, and for the stability in the centroids obtained. To determine the most appropriate number

of clusters, we employed the inter-pattern correlation variance (IPCV) as the primary method, as we are mainly interested in the centroids' aspect, supplemented by the elbow method for confirmation.

The IPCV is computed by vectorizing the set of centroids for a given k and calculating the variance of Pearson correlations between each pair of centroids (Demertzi et al., 2019). The optimal k, indicating the number of clusters, is determined by identifying the maximum value of this metric. To validate this optimal k, we employed the elbow method, which is typically based on the within-cluster sum of squares differences. While the elbow was not always as distinctly observable as desired, it still often coincided with the proposed *k* from the IPCV.

Structure-Function Correlation

To investigate the dependence of brain dynamics on the state of consciousness, we defined a measure of similarity between functional and structural connectivity. We resorted to a widely used group estimate of macaque anatomical connectivity provided by the CoCoMac 2.0 database. We computed the linear correlation coefficient between the entries of both matrices (k-means centroids and anatomical connectome) for each set of k-clusters. This was performed for each phase-based coordination pattern obtained using the k-means algorithm and was denoted structure-function correlation (SFC). We then reorganized the patterns' labels, their unique associated integer between 1 and k, such that the new 'first' pattern would be the pattern with the lowest SFC, and the 'k^{th}' pattern the one with the highest correlation to the anatomy (i.e. structure). Last, we computed the linear slope coefficient of the relationship between the occurrence rate of each centroid and the corresponding centroid/anatomical correlation (i.e. the SFC) to establish a possible tendency for functional states with higher (or lower) correlation to the anatomy.

Brain States' Presence Rate Distribution and Shannon Entropy

For each condition, we computed the histogram associated with the total time of visits of each pattern. This histogram, after normalization, corresponds to the probability distribution of the patterns' occurrence. For each of the normalized histogram of occurrence, and each value of k in the k-means algorithm, we obtained the Shannon entropy (Shannon 1948) as follows:

$$S = -\sum_i P_i \log_2 P_i \qquad (5)$$

Where P_i is the probability (normalized histogram) of visit for each pattern in each brain state (condition).

Markov Chain

For every TR, the k-means algorithm assigns the index of the closest centroid to the corresponding empirical phase coherence matrix, resulting in a sequence of indexes (integers, between 1 and k). We reckon the sequence of "patterns visited" as a sequence of random variables that jumps from one pattern to another pattern with a certain probability given by the empirical frequencies in which these transitioning events happen in the sequence. From these empirical frequencies, we built a Markov Chain, as done previously (Demertzi et al., 2019). More

specifically, we counted the number of transitions between all pairs of patterns without considering self-transitions (which correspond to remaining in the same pattern) and normalized these counts to obtain a Markov transition probability matrix $\mathbf{P}$.

Statistical Analysis

To assess the statistical significance of comparing different conditions and differences in occurrence rates, slopes' coefficient, and Shannon entropy, we performed independent t-test with Bonferonni correction between the awake and anesthesia conditions before any stimulation and all their associated stimulation conditions and reported the associated *p* values. We also performed three or two-way ANOVA to confirm that the obtained results of comparing two conditions together (with corrections for multiple comparisons) are consistent with comparing the conditions given the independent variables at play: during/after stimulation, amperage/montage used, and the animal ; and to evaluate possible interactions between said variables.

All these analyses are shown in table form (Table 4) following APA standards by reporting the means and standard deviations, the statistics (T-values or F-values), the degrees of freedom and the *p* values, all to two significant digits. For the ANOVA tests, we also report the sum of squares.

To ensure the reliability of the transition probabilities, we performed a bootstrap method that breaks the temporal dependencies in the chain of visited states. We randomized the order of brain states' appearance, thus conserving the overall statistics but breaking the temporal dependence between specific pairs of visited states. We performed this randomization 10.000 times per condition and computed as many transition matrices. We asserted that certain states' transitions truly reflected a stochastic process and were hence not due to chance by verifying if the empirical transition matrices were above the confidence interval defined by successively stricter confidence levels: 90%, 95%, and 99%. This also allows us to somewhat compensate for the animal-specific effects by discarding them. Finally, for the transitions that did pass at least the 90% confidence interval test, we compared, using independent t-tests with Bonferonni correction, the transition probabilities between conditions and reported the associated *p* values.

All these analyses were performed using customized codes available on an open Github repository for transparency, reproducibility, and open-science (https://github.com/Krigsa/phase_coherence_kmeans). Known Python libraries such as *add_state_annot* (Charlier et al., 2022) or *Scipy* (Virtanen et al., 2020) were used to perform the statistical analysis notably.

ACKNOWLEDGEMENTS.

The research was supported by the Institut National de la Santé et de la Recherche Médicale (to G.H. and B.J.), the Fondation pour la Recherche Médicale (FRM grant number ECO20160736100, to J.T.), FNRS Belgium (project MIS/VA - F.4523.21, to C.M.S.), grant Embodied-Time (40011405, to C.M.S.), Centre National de la Recherche Scientifique and the European Community (Human Brain Project, H2020-945538, to A.D. and R.C.), the Fondation Bettencourt Schueller (to B.J.), Fondation de France (to B.J.), Human Brain Project (Corticity project FLAC-ERA JTC2017, to B.J.), UVSQ (to B.J.), Commissariat à l'Energie Atomique (to B.J.), Collège de France (to B.J.).

References

Alam, Mahtab, Dennis Q. Truong, Niranjan Khadka, and Marom Bikson. 2016. “Spatial and Polarity Precision of Concentric High-Definition Transcranial Direct Current Stimulation (HD-tDCS).” *Physics in Medicine and Biology* 61 (12): 4506–21.

Alfonsi, Valentina, Aurora D’Atri, Serena Scarpelli, Maurizio Gorgoni, Francesco Giacinti, Ludovica Annarumma, Federico Salfi, Giulia Amicucci, Domenico Corigliano, and Luigi De Gennaro. 2023. “The Effects of Bifrontal Anodal Transcranial Direct Current Stimulation (tDCS) on Sleepiness and Vigilance in Partially Sleep-Deprived Subjects: A Multidimensional Study.” *Journal of Sleep Research* 32 (4): e13869.

Allen, Elena A., Eswar Damaraju, Sergey M. Plis, Erik B. Erhardt, Tom Eichele, and Vince D. Calhoun. 2014. “Tracking Whole-Brain Connectivity Dynamics in the Resting State.” *Cerebral Cortex* 24 (3): 663–76.

Alonso Martínez, Sonsoles, Gustavo Deco, Gert J. Ter Horst, and Joana Cabral. 2020. “The Dynamics of Functional Brain Networks Associated With Depressive Symptoms in a Nonclinical Sample.” *Frontiers in Neural Circuits* 14 (September):570583.

Angelakis, Efthymios, Evangelia Liouta, Nikos Andreadis, Stephanos Korfias, Periklis Ktonas, George Stranjalis, and Damianos E. Sakas. 2014. “Transcranial Direct Current Stimulation Effects in Disorders of Consciousness.” *Archives of Physical Medicine and Rehabilitation* 95 (2): 283–89.

Annarumma, Ludovica, Aurora D’Atri, Valentina Alfonsi, and Luigi De Gennaro. 2018. “The Efficacy of Transcranial Current Stimulation Techniques to Modulate Resting-State EEG, to Affect Vigilance and to Promote Sleepiness.” *Brain Sciences* 8 (7). https://doi.org/10.3390/brainsci8070137.

Antal, Andrea, Daniella Terney, Csaba Poreisz, and Walter Paulus. 2007. “Towards Unravelling Task-Related Modulations of Neuroplastic Changes Induced in the Human Motor Cortex.” *The European Journal of Neuroscience* 26 (9): 2687–91.

Axelrod, Vadim, Geraint Rees, Michal Lavidor, and Moshe Bar. 2015. “Increasing Propensity to Mind-Wander with Transcranial Direct Current Stimulation.” *Proceedings of the National Academy of Sciences of the United States of America* 112 (11): 3314–19.

Bai, Yang, Xiaoyu Xia, Jiannan Kang, Yi Yang, Jianghong He, and Xiaoli Li. 2017. “TDCS Modulates Cortical Excitability in Patients with Disorders of Consciousness.” *NeuroImage. Clinical* 15 (January):702–9.

Bai, Yang, Xiaoyu Xia, Yong Wang, Yongkun Guo, Yi Yang, Jianghong He, and Xiaoli Li. 2018. “Fronto-Parietal Coherence Response to tDCS Modulation in Patients with Disorders of Consciousness.” *The International Journal of Neuroscience* 128 (7): 587–94.

Baker, Adam P., Matthew J. Brookes, Iead A. Rezek, Stephen M. Smith, Timothy Behrens, Penny J. Probert Smith, and Mark Woolrich. 2014. “Fast Transient Networks in Spontaneous Human Brain Activity.” *eLife* 3 (March):e01867.

Bakker, Rembrandt, Thomas Wachtler, and Markus Diesmann. 2012. “CoCoMac 2.0 and the Future of Tract-Tracing Databases.” *Frontiers in Neuroinformatics* 6 (December):30.

Barttfeld, Pablo, Lynn Uhrig, Jacobo D. Sitt, Mariano Sigman, Béchir Jarraya, and Stanislas Dehaene. 2015. “Signature of Consciousness in the Dynamics of Resting-State Brain Activity.” *Proceedings of the National Academy of Sciences of the United States of America* 112 (3): 887–92.

Bekinschtein, Tristan A., Stanislas Dehaene, Benjamin Rohaut, François Tadel, Laurent Cohen, and Lionel Naccache. 2009. “Neural Signature of the Conscious Processing of Auditory Regularities.” *Proceedings of the National Academy of Sciences of the United States of America* 106 (5): 1672–77.

Bikson, Marom, Masashi Inoue, Hiroki Akiyama, Jackie K. Deans, John E. Fox, Hiroyoshi Miyakawa, and John G. R. Jefferys. 2004. “Effects of Uniform Extracellular DC Electric Fields on Excitability in Rat Hippocampal Slices in Vitro.” *The Journal of Physiology* 557 (Pt 1): 175–90.

Bikson, Marom, Author Name, and Asif Rahman. 2013. “Origins of Specificity during tDCS: Anatomical, Activity-Selective, and Input-Bias Mechanisms.” *Frontiers in Human*

Neuroscience 7 (October):688.
Bodien, Yelena G., Judith Allanson, Paolo Cardone, Arthur Bonhomme, Jerina Carmona, Camille Chatelle, Srivas Chennu, et al., 2024. “Cognitive Motor Dissociation in Disorders of Consciousness.” *The New England Journal of Medicine* 391 (7): 598–608.
Boly, M., C. Phillips, L. Tshibanda, A. Vanhaudenhuyse, M. Schabus, T. T. Dang-Vu, G. Moonen, R. Hustinx, P. Maquet, and S. Laureys. 2008. “Intrinsic Brain Activity in Altered States of Consciousness: How Conscious Is the Default Mode of Brain Function?” *Annals of the New York Academy of Sciences* 1129:119–29.
Bracewell, Ronald Newbold. 2000. *The Fourier Transform and Its Applications*. McGraw Hill.
Cabral, Joana, Diego Vidaurre, Paulo Marques, Ricardo Magalhães, Pedro Silva Moreira, José Miguel Soares, Gustavo Deco, Nuno Sousa, and Morten L. Kringelbach. 2017. “Cognitive Performance in Healthy Older Adults Relates to Spontaneous Switching between States of Functional Connectivity during Rest.” *Scientific Reports* 7 (1): 5135.
Calhoun, Vince D., Robyn Miller, Godfrey Pearlson, and Tulay Adalı. 2014. “The Chronnectome: Time-Varying Connectivity Networks as the next Frontier in fMRI Data Discovery.” *Neuron* 84 (2): 262–74.
Castro, Pablo, Luppi, Andrea, Tagliazucchi, Enzo, Perl, Yonatan S., Naci, Lorina, Owen, Adrian M., Sitt, Jacobo D., Destexhe, Alain, Cofré, Rodrigo. 2024. “Dynamical Structure-Function Correlations Provide Robust and Generalizable Signatures of Consciousness in Humans.” *Commun Biol* 7 (1): 1224.
Cavinato, Marianna, Clara Genna, Emanuela Formaggio, Caterina Gregorio, Silvia F. Storti, Paolo Manganotti, Emanuela Casanova, Roberto Piperno, and Francesco Piccione. 2019. “Behavioural and Electrophysiological Effects of tDCS to Prefrontal Cortex in Patients with Disorders of Consciousness.” *Clinical Neurophysiology : Official Journal of the International Federation of Clinical Neurophysiology* 130 (2): 231–38.
Charlier, Florian, Marc Weber, Dariusz Izak, Emerson Harkin, Marcin Magnus, Joseph Lalli, Louison Fresnais, et al., 2022. *Trevismd/statannotations: v0.5*. Zenodo. https://doi.org/10.5281/ZENODO.7213391.
Coulborn, Sean, and Davinia Fernández-Espejo. 2022. “Prefrontal tDCS Is Unable to Modulate Mind Wandering Propensity or Underlying Functional or Effective Brain Connectivity.” *Scientific Reports* 12 (1): 18021.
Crone, Julia S., Evan S. Lutkenhoff, Paul M. Vespa, and Martin M. Monti. 2020. “A Systematic Investigation of the Association between Network Dynamics in the Human Brain and the State of Consciousness.” *Neuroscience of Consciousness* 2020 (1): niaa008.
Dai, Jing, Hang Wang, Lin Yang, Chunchen Wang, Shan Cheng, Taihui Zhang, Jin Ma, Zhihong Wen, Xinsheng Cao, and Wendong Hu. 2022. “The Neuroelectrophysiological and Behavioral Effects of Transcranial Direct Current Stimulation on Executive Vigilance under a Continuous Monotonous Condition.” *Frontiers in Neuroscience* 16 (September):910457.
Dalong, Guo, Li Jiyuan, Zhang Ying, Zha Lei, Hou Yanhong, and Shao Yongcong. 2020. “Transcranial Direct Current Stimulation Reconstructs Diminished Thalamocortical Connectivity during Prolonged Resting Wakefulness: A Resting-State fMRI Pilot Study.” *Brain Imaging and Behavior* 14 (1): 278–88.
Damoiseaux, J. S., S. A. R. B. Rombouts, F. Barkhof, P. Scheltens, C. J. Stam, S. M. Smith, and C. F. Beckmann. 2006. “Consistent Resting-State Networks across Healthy Subjects.” *Proceedings of the National Academy of Sciences of the United States of America* 103 (37): 13848–53.
Datta, Abhishek, Varun Bansal, Julian Diaz, Jinal Patel, Davide Reato, and Marom Bikson. 2009. “Gyri-Precise Head Model of Transcranial Direct Current Stimulation: Improved Spatial Focality Using a Ring Electrode versus Conventional Rectangular Pad.” *Brain Stimulation* 2 (4): 201–7, 207.e1.
Datta, Abhishek, Matthew R. Krause, Praveen K. Pilly, Jaehoon Choe, Theodoras P. Zanos, Chris Thomas, and Christopher C. Pack. 2016. “On Comparing in Vivo Intracranial Recordings in Non-Human Primates to Predictions of Optimized Transcranial Electrical Stimulation.” *Annual International Conference of the IEEE Engineering in Medicine and Biology Society. IEEE Engineering in Medicine and Biology Society. Annual International Conference* 2016

(August):1774–77.
Deco, Gustavo, Viktor K. Jirsa, and Anthony R. McIntosh. 2011. “Emerging Concepts for the Dynamical Organization of Resting-State Activity in the Brain.” *Nature Reviews. Neuroscience* 12 (1): 43–56.
Deco, Gustavo, Viktor K. Jirsa, and Anthony R. McIntosh. 2013. “Resting Brains Never Rest: Computational Insights into Potential Cognitive Architectures.” *Trends in Neurosciences* 36 (5): 268–74.
Demertzi, A., E. Tagliazucchi, S. Dehaene, G. Deco, P. Barttfeld, F. Raimondo, C. Martial, et al., 2019. “Human Consciousness Is Supported by Dynamic Complex Patterns of Brain Signal Coordination.” *Science Advances* 5 (2): eaat7603.
Ensel, Scott, Lynn Uhrig, Ayberk Ozkirli, Guylaine Hoffner, Jordy Tasserie, Stanislas Dehaene, Dimitri Van De Ville, Béchir Jarraya, and Elvira Pirondini. 2023. “Transient Brain Activity Dynamics Discriminate Levels of Consciousness during Anesthesia.” *bioRxiv*. https://doi.org/10.1101/2023.10.09.560209.
Fonteneau, Clara, Marine Mondino, Martijn Arns, Chris Baeken, Marom Bikson, Andre R. Brunoni, Matthew J. Burke, et al., 2019. “Sham tDCS: A Hidden Source of Variability? Reflections for Further Blinded, Controlled Trials.” *Brain Stimulation* 12 (3): 668–73.
Fox, Michael D., Maurizio Corbetta, Abraham Z. Snyder, Justin L. Vincent, and Marcus E. Raichle. 2006. “Spontaneous Neuronal Activity Distinguishes Human Dorsal and Ventral Attention Systems.” *Proceedings of the National Academy of Sciences of the United States of America* 103 (26): 10046–51.
Frase, Lukas, Jonathan G. Maier, Sulamith Zittel, Tobias Freyer, Dieter Riemann, Claus Normann, Bernd Feige, Michael A. Nitsche, and Christoph Nissen. 2015. “Bifrontal Anodal Transcranial Direct Current Stimulation (tDCS) Improves Daytime Vigilance and Sleepiness in a Patient With Organic Hypersomnia Following Reanimation.” *Brain Stimulation* 8 (4): 844–46.
Frase, Lukas, Hannah Piosczyk, Sulamith Zittel, Friederike Jahn, Peter Selhausen, Lukas Krone, Bernd Feige, et al., 2016. “Modulation of Total Sleep Time by Transcranial Direct Current Stimulation (tDCS).” *Neuropsychopharmacology: Official Publication of the American College of Neuropsychopharmacology* 41 (10): 2577–86.
Frey, Stephen, Deepak N. Pandya, M. Mallar Chakravarty, Lara Bailey, Michael Petrides, and D. Louis Collins. 2011. “An MRI Based Average Macaque Monkey Stereotaxic Atlas and Space (MNI Monkey Space).” *NeuroImage* 55 (4): 1435–42.
Glerean, Enrico, Juha Salmi, Juha M. Lahnakoski, Iiro P. Jääskeläinen, and Mikko Sams. 2012. “Functional Magnetic Resonance Imaging Phase Synchronization as a Measure of Dynamic Functional Connectivity.” *Brain Connectivity* 2 (2): 91–101.
Golkowski, Daniel, Stephen Karl Larroque, Audrey Vanhaudenhuyse, Alain Plenevaux, Melanie Boly, Carol Di Perri, Andreas Ranft, et al., 2019. “Changes in Whole Brain Dynamics and Connectivity Patterns during Sevoflurane- and Propofol-Induced Unconsciousness Identified by Functional Magnetic Resonance Imaging.” *Anesthesiology* 130 (6): 898–911.
Guidetti, Matteo, Mattia Arlotti, Tommaso Bocci, Anna Maria Bianchi, Marta Parazzini, Roberta Ferrucci, and Alberto Priori. 2022. “Electric Fields Induced in the Brain by Transcranial Electric Stimulation: A Review of In Vivo Recordings.” *Biomedicines* 10 (10). https://doi.org/10.3390/biomedicines10102333.
Guo, Yongkun, Yang Bai, Xiaoyu Xia, Jinju Li, Xiaoli Wang, Yiwu Dai, Yuanyuan Dang, Jianghong He, Chunying Liu, and Hui Zhang. 2019. “Effects of Long-Lasting High-Definition Transcranial Direct Current Stimulation in Chronic Disorders of Consciousness: A Pilot Study.” *Frontiers in Neuroscience* 13 (April):412.
Gu, Zhongke, Wenxiang Chen, Qian Lu, Jiansong Dai, Shugang Hu, Kai Xu, Yao Geng, et al., 2022. “Anodal High-Definition Transcranial Direct Current Stimulation Reduces Heart Rate and Modulates Heart-Rate Variability in Healthy Young People: A Randomized Cross-Controlled Trial.” *Frontiers in Cardiovascular Medicine* 9 (December):1070157.
Havlík, Marek, Jaroslav Hlinka, Monika Klírová, Petr Adámek, and Jiří Horáček. 2023. “Towards Causal Mechanisms of Consciousness through Focused Transcranial Brain Stimulation.” *Neuroscience of Consciousness* 2023 (1): niad008.

Hermann, Bertrand, Federico Raimondo, Lukas Hirsch, Yu Huang, Mélanie Denis-Valente, Pauline Pérez, Denis Engemann, et al., 2020. “Combined Behavioral and Electrophysiological Evidence for a Direct Cortical Effect of Prefrontal tDCS on Disorders of Consciousness.” *Scientific Reports* 10 (1): 4323.

Hindriks, R., M. H. Adhikari, Y. Murayama, M. Ganzetti, D. Mantini, N. K. Logothetis, and G. Deco. 2016. “Can Sliding-Window Correlations Reveal Dynamic Functional Connectivity in Resting-State fMRI?” *NeuroImage* 127 (February):242–56.

Hsu, Gavin, A. Duke Shereen, Leonardo G. Cohen, and Lucas C. Parra. 2023. “Robust Enhancement of Motor Sequence Learning with 4 mA Transcranial Electric Stimulation.” *Brain Stimulation* 16 (1): 56–67.

Huang, Wangshan, Sarah Wannez, Felipe Fregni, Xiaohua Hu, Shan Jing, Geraldine Martens, Minhui He, Haibo Di, Steven Laureys, and Aurore Thibaut. 2017. “Repeated Stimulation of the Posterior Parietal Cortex in Patients in Minimally Conscious State: A Sham-Controlled Randomized Clinical Trial.” *Brain Stimulation* 10 (3): 718–20.

Huang, Yu, Yuzhuo Su, Christopher Rorden, Jacek Dmochowski, Abhishek Datta, and Lucas C. Parra. 2012. “An Automated Method for High-Definition Transcranial Direct Current Stimulation Modeling.” *Conference Proceedings: ... Annual International Conference of the IEEE Engineering in Medicine and Biology Society. IEEE Engineering in Medicine and Biology Society. Conference* 2012:5376–79.

Huang, Zirui, Jun Zhang, Jinsong Wu, George A. Mashour, and Anthony G. Hudetz. 2020. “Temporal Circuit of Macroscale Dynamic Brain Activity Supports Human Consciousness.” *Science Advances* 6 (11): eaaz0087.

Jamil, Asif, Giorgi Batsikadze, Hsiao-I Kuo, Ludovica Labruna, Alkomiet Hasan, Walter Paulus, and Michael A. Nitsche. 2017. “Systematic Evaluation of the Impact of Stimulation Intensity on Neuroplastic after-Effects Induced by Transcranial Direct Current Stimulation.” *The Journal of Physiology* 595 (4): 1273–88.

Jamil, Asif, Giorgi Batsikadze, Hsiao-I Kuo, Raf L. J. Meesen, Peter Dechent, Walter Paulus, and Michael A. Nitsche. 2020. “Current Intensity- and Polarity-Specific Online and Aftereffects of Transcranial Direct Current Stimulation: An fMRI Study.” *Human Brain Mapping* 41 (6): 1644–66.

Karahanoğlu, Fikret Işik, and Dimitri Van De Ville. 2015. “Transient Brain Activity Disentangles fMRI Resting-State Dynamics in Terms of Spatially and Temporally Overlapping Networks.” *Nature Communications* 6 (July):7751.

Kato, Risako, and Ken Solt. 2021. “Prehabilitation With Brain Stimulation?” *Anesthesia and Analgesia* 132 (5): 1344–46.

Kelz, Max B., and George A. Mashour. 2019. “The Biology of General Anesthesia from Paramecium to Primate.” *Current Biology : CB* 29 (22): R1199–1210.

Kötter, Rolf, and Egon Wanke. 2005. “Mapping Brains without Coordinates.” *Philosophical Transactions of the Royal Society of London. Series B, Biological Sciences* 360 (1456): 751–66.

Krone, Lukas, Lukas Frase, Hannah Piosczyk, Peter Selhausen, Sulamith Zittel, Friederike Jahn, Marion Kuhn, et al., 2017. “Top-down Control of Arousal and Sleep: Fundamentals and Clinical Implications.” *Sleep Medicine Reviews* 31 (February):17–24.

Lee, Won Hee, Sarah H. Lisanby, Andrew F. Laine, and Angel V. Peterchev. 2015. “Electric Field Model of Transcranial Electric Stimulation in Nonhuman Primates: Correspondence to Individual Motor Threshold.” *IEEE Transactions on Bio-Medical Engineering* 62 (9): 2095–2105.

Lefaucheur, Jean-Pascal, Andrea Antal, Samar S. Ayache, David H. Benninger, Jérôme Brunelin, Filippo Cogiamanian, Maria Cotelli, et al., 2017. “Evidence-Based Guidelines on the Therapeutic Use of Transcranial Direct Current Stimulation (tDCS).” *Clinical Neurophysiology: Official Journal of the International Federation of Clinical Neurophysiology* 128 (1): 56–92.

Lefaucheur, Jean-Pascal, and Fabrice Wendling. 2019. “Mechanisms of Action of tDCS: A Brief and Practical Overview.” *Neurophysiologie Clinique = Clinical Neurophysiology* 49 (4): 269–75.

Li, Lucia M., Ines R. Violante, Rob Leech, Ewan Ross, Adam Hampshire, Alexander Opitz, John C. Rothwell, David W. Carmichael, and David J. Sharp. 2019. “Brain State and Polarity Dependent Modulation of Brain Networks by Transcranial Direct Current Stimulation.” *Human Brain Mapping* 40 (3): 904–15.

Liu, Zhenyu, Xintong Zhang, Binbin Yu, Jiayue Wang, and Xiao Lu. 2023. “Effectiveness on Level of Consciousness of Non-Invasive Neuromodulation Therapy in Patients with Disorders of Consciousness: A Systematic Review and Meta-Analysis.” *Frontiers in Human Neuroscience* 17 (May):1129254.

Louviot, Samuel, Louise Tyvaert, Louis G. Maillard, Sophie Colnat-Coulbois, Jacek Dmochowski, and Laurent Koessler. 2022. “Transcranial Electrical Stimulation Generates Electric Fields in Deep Human Brain Structures.” *Brain Stimulation* 15 (1): 1–12.

Luppi, Andrea I. 2024. “What Anaesthesia Reveals about Human Brains and Consciousness.” *Nature Human Behaviour* 8 (5): 801–4.

Luppi, Andrea I., Daniel Golkowski, Andreas Ranft, Rüdiger Ilg, Denis Jordan, David K. Menon, and Emmanuel A. Stamatakis. 2021. “Brain Network Integration Dynamics Are Associated with Loss and Recovery of Consciousness Induced by Sevoflurane.” *Human Brain Mapping* 42 (9): 2802–22.

Luppi, Andrea I., Lynn Uhrig, Jordy Tasserie, Camilo M. Signorelli, Emmanuel A. Stamatakis, Alain Destexhe, Bechir Jarraya, and Rodrigo Cofre. 2024. “Local Orchestration of Distributed Functional Patterns Supporting Loss and Restoration of Consciousness in the Primate Brain.” *Nature Communications* 15 (1): 2171.

Maeoka, Hiroshi, Atsushi Matsuo, Makoto Hiyamizu, Shu Morioka, and Hiroshi Ando. 2012. “Influence of Transcranial Direct Current Stimulation of the Dorsolateral Prefrontal Cortex on Pain Related Emotions: A Study Using Electroencephalographic Power Spectrum Analysis.” *Neuroscience Letters* 512 (1): 12–16.

Mansouri, Mohammad Taghi, and Paul S. García. 2021. “Repetitive Anodal Transcranial Direct Current Stimulation Hastens Isoflurane-Induced Emergence and Recovery and Enhances Memory in Healthy Rats.” *Anesthesia and Analgesia* 132 (5): 1347–58.

Mantell, Kathleen E., Nipun D. Perera, Sina Shirinpour, Oula Puonti, Ting Xu, Jan Zimmermann, Arnaud Falchier, Sarah R. Heilbronner, Axel Thielscher, and Alexander Opitz. 2023. “Anatomical Details Affect Electric Field Predictions for Non-Invasive Brain Stimulation in Non-Human Primates.” *NeuroImage* 279 (October):120343.

Martens, Géraldine, Felipe Fregni, Manon Carrière, Alice Barra, Steven Laureys, and Aurore Thibaut. 2019. “Single tDCS Session of Motor Cortex in Patients with Disorders of Consciousness: A Pilot Study.” *Brain Injury* 33 (13-14): 1679–83.

Martens, Géraldine, Nicolas Lejeune, Anthony Terrence O’Brien, Felipe Fregni, Charlotte Martial, Sarah Wannez, Steven Laureys, and Aurore Thibaut. 2018. “Randomized Controlled Trial of Home-Based 4-Week tDCS in Chronic Minimally Conscious State.” *Brain Stimulation* 11 (5): 982–90.

Mashour, George A., Dinesh Pal, and Emery N. Brown. 2022. “Prefrontal Cortex as a Key Node in Arousal Circuitry.” *Trends in Neurosciences* 45 (10): 722–32.

McCormick, D. A. 1992. “Neurotransmitter Actions in the Thalamus and Cerebral Cortex and Their Role in Neuromodulation of Thalamocortical Activity.” *Progress in Neurobiology* 39 (4): 337–88.

McIntire, Lindsey K., R. Andy McKinley, Chuck Goodyear, and Justin Nelson. 2014. “A Comparison of the Effects of Transcranial Direct Current Stimulation and Caffeine on Vigilance and Cognitive Performance during Extended Wakefulness.” *Brain Stimulation* 7 (4): 499–507.

Mensen, Armand, Olivier Bodart, Aurore Thibaut, Sarah Wannez, Jitka Annen, Steven Laureys, and Olivia Gosseries. 2020. “Decreased Evoked Slow-Activity After tDCS in Disorders of Consciousness.” *Frontiers in Systems Neuroscience* 14 (September):62.

Milham, Michael P., Lei Ai, Bonhwang Koo, Ting Xu, Céline Amiez, Fabien Balezeau, Mark G. Baxter, et al., 2018. “An Open Resource for Non-Human Primate Imaging.” *Neuron* 100 (1): 61–74.e2.

Monte-Silva, Katia, Min-Fang Kuo, David Liebetanz, Walter Paulus, and Michael A. Nitsche.

2010. “Shaping the Optimal Repetition Interval for Cathodal Transcranial Direct Current Stimulation (tDCS).” *Journal of Neurophysiology* 103 (4): 1735–40.
Monti, Martin M., Audrey Vanhaudenhuyse, Martin R. Coleman, Melanie Boly, John D. Pickard, Luaba Tshibanda, Adrian M. Owen, and Steven Laureys. 2010. “Willful Modulation of Brain Activity in Disorders of Consciousness.” *The New England Journal of Medicine* 362 (7): 579–89.
Mortaheb, Sepehr, Laurens Van Calster, Federico Raimondo, Manousos A. Klados, Paradeisios Alexandros Boulakis, Kleio Georgoula, Steve Majerus, Dimitri Van De Ville, and Athena Demertzi. 2022. “Mind Blanking Is a Distinct Mental State Linked to a Recurrent Brain Profile of Globally Positive Connectivity during Ongoing Mentation.” *Proceedings of the National Academy of Sciences of the United States of America* 119 (41): e2200511119.
Narmashiri, Abdolvahed, and Fatemeh Akbari. 2023. “The Effects of Transcranial Direct Current Stimulation (tDCS) on the Cognitive Functions: A Systematic Review and Meta-Analysis.” *Neuropsychology Review*, December. https://doi.org/10.1007/s11065-023-09627-x.
Nawani, Hema, Matthias Mittner, and Gábor Csifcsák. 2023. “Modulation of Mind Wandering Using Transcranial Direct Current Stimulation: A Meta-Analysis Based on Electric Field Modeling.” *NeuroImage* 272 (May):120051.
Nitsche, M. A., and W. Paulus. 2000. “Excitability Changes Induced in the Human Motor Cortex by Weak Transcranial Direct Current Stimulation.” *The Journal of Physiology* 527 Pt 3 (Pt 3): 633–39.
Nitsche, Michael A., and Marom Bikson. 2017. “Extending the Parameter Range for tDCS: Safety and Tolerability of 4 mA Stimulation.” *Brain Stimulation* 10 (3): 541–42.
Owen, Adrian M., Martin R. Coleman, Melanie Boly, Matthew H. Davis, Steven Laureys, and John D. Pickard. 2006. “Detecting Awareness in the Vegetative State.” *Science (New York, N.Y.)* 313 (5792): 1402.
Panagiotaropoulos, Theofanis I. 2024. “An Integrative View of the Role of Prefrontal Cortex in Consciousness.” *Neuron* 112 (10): 1626–41.
Patel, Shaun R., Jesus J. Ballesteros, Omar J. Ahmed, Pamela Huang, Jessica Briscoe, Emad N. Eskandar, and Yumiko Ishizawa. 2020. “Dynamics of Recovery from Anaesthesia-Induced Unconsciousness across Primate Neocortex.” *Brain: A Journal of Neurology* 143 (3): 833–43.
Peng, Yuan, Jingpu Zhao, Xiao Lu, Juntao Dong, Shunxi Zhang, Jin Zhang, Huihua Liu, et al., 2022. “Efficacy of Transcranial Direct Current Stimulation Over Dorsolateral Prefrontal Cortex in Patients With Minimally Conscious State.” *Frontiers in Neurology* 13 (February):821286.
Perri, Rinaldo Livio, and Gloria Di Filippo. 2023. “Alteration of Hypnotic Experience Following Transcranial Electrical Stimulation of the Left Prefrontal Cortex.” *International Journal of Clinical and Health Psychology: IJCHP* 23 (2): 100346.
Perri, Rinaldo L., Davide Perrotta, Francesco Rossani, and Ronald J. Pekala. 2022. “Boosting the Hypnotic Experience. Inhibition of the Dorsolateral Prefrontal Cortex Alters Hypnotizability and Sense of Agency. A Randomized, Double-Blind and Sham-Controlled tDCS Study.” *Behavioural Brain Research* 425 (May):113833.
Polanía, Rafael, Walter Paulus, and Michael A. Nitsche. 2012. “Modulating Cortico-Striatal and Thalamo-Cortical Functional Connectivity with Transcranial Direct Current Stimulation.” *Human Brain Mapping* 33 (10): 2499–2508.
Preti, Maria Giulia, Thomas Aw Bolton, and Dimitri Van De Ville. 2017. “The Dynamic Functional Connectome: State-of-the-Art and Perspectives.” *NeuroImage* 160 (October):41–54.
Raichle, M. E., A. M. MacLeod, A. Z. Snyder, W. J. Powers, D. A. Gusnard, and G. L. Shulman. 2001. “A Default Mode of Brain Function.” *Proceedings of the National Academy of Sciences of the United States of America* 98 (2): 676–82.
Rebollo, Beatriz, Bartosz Telenczuk, Alvaro Navarro-Guzman, Alain Destexhe, and Maria V. Sanchez-Vives. 2021. “Modulation of Intercolumnar Synchronization by Endogenous Electric Fields in Cerebral Cortex.” *Science Advances* 7 (10). https://doi.org/10.1126/sciadv.abc7772.
Redinbaugh, Michelle J., Jessica M. Phillips, Niranjan A. Kambi, Sounak Mohanta, Samantha Andryk, Gaven L. Dooley, Mohsen Afrasiabi, Aeyal Raz, and Yuri B. Saalmann. 2020. “Thalamus Modulates Consciousness via Layer-Specific Control of Cortex.” *Neuron* 106 (1):

66–75.e12.
Rodrigues, Bruno, Catarina A. Barboza, Eliezer G. Moura, Gabriela Ministro, Silvia E. Ferreira-Melo, Javier B. Castaño, Wilton M. S. Nunes, et al., 2022. “Acute and Short-Term Autonomic and Hemodynamic Responses to Transcranial Direct Current Stimulation in Patients With Resistant Hypertension.” *Frontiers in Cardiovascular Medicine* 9 (March):853427.
Saturnino, Guilherme B., Oula Puonti, Jesper D. Nielsen, Daria Antonenko, Kristoffer H. Madsen, and Axel Thielscher. 2019. “SimNIBS 2.1: A Comprehensive Pipeline for Individualized Electric Field Modelling for Transcranial Brain Stimulation.” In *Brain and Human Body Modeling: Computational Human Modeling at EMBC 2018*, edited by Sergey Makarov, Marc Horner, and Gregory Noetscher. Cham (CH): Springer.
Sdoia, Stefano, David Conversi, Anna Pecchinenda, and Fabio Ferlazzo. 2019. “Access to Consciousness of Briefly Presented Visual Events Is Modulated by Transcranial Direct Current Stimulation of Left Dorsolateral Prefrontal Cortex.” *Scientific Reports* 9 (1): 10950.
Shannon, C. E. 1948. *A mathematical theory of communication*.
Shen, Kelly, Gleb Bezgin, Michael Schirner, Petra Ritter, Stefan Everling, and Anthony R. McIntosh. 2019. “A Macaque Connectome for Large-Scale Network Simulations in TheVirtualBrain.” *Scientific Data* 6 (1): 123.
Signorelli, Camilo Miguel, Lynn Uhrig, Morten Kringelbach, Bechir Jarraya, and Gustavo Deco. 2021. “Hierarchical Disruption in the Cortex of Anesthetized Monkeys as a New Signature of Consciousness Loss.” *NeuroImage* 227 (February):117618.
Steriade, Mircea M., and Robert W. McCarley. 2013. *Brainstem Control of Wakefulness and Sleep*. Springer Science & Business Media.
Straudi, Sofia, Valentina Bonsangue, Sonia Mele, Laila Craighero, Andrea Montis, Felipe Fregni, Susanna Lavezzi, and Nino Basaglia. 2019. “Bilateral M1 Anodal Transcranial Direct Current Stimulation in Post Traumatic Chronic Minimally Conscious State: A Pilot EEG-tDCS Study.” *Brain Injury* 33 (4): 490–95.
Tagliazucchi, Enzo, and Helmut Laufs. 2014. “Decoding Wakefulness Levels from Typical fMRI Resting-State Data Reveals Reliable Drifts between Wakefulness and Sleep.” *Neuron* 82 (3): 695–708.
Tasserie, Jordy, Lynn Uhrig, Jacobo D. Sitt, Dragana Manasova, Morgan Dupont, Stanislas Dehaene, and Béchir Jarraya. 2022. “Deep Brain Stimulation of the Thalamus Restores Signatures of Consciousness in a Nonhuman Primate Model.” *Science Advances* 8 (11): eabl5547.
Thibaut, Aurore, Marie-Aurélie Bruno, Didier Ledoux, Athena Demertzi, and Steven Laureys. 2014. “tDCS in Patients with Disorders of Consciousness: Sham-Controlled Randomized Double-Blind Study.” *Neurology* 82 (13): 1112–18.
Thibaut, Aurore, Felipe Fregni, Anna Estraneo, Salvatore Fiorenza, Enrique Noe, Roberto Llorens, Joan Ferri, et al., 2023. “Sham-Controlled Randomized Multicentre Trial of Transcranial Direct Current Stimulation for Prolonged Disorders of Consciousness.” *European Journal of Neurology* 30 (10): 3016–31.
Thibaut, Aurore, Nicholas Schiff, Joseph Giacino, Steven Laureys, and Olivia Gosseries. 2019. “Therapeutic Interventions in Patients with Prolonged Disorders of Consciousness.” *The Lancet. Neurology* 18 (6): 600–614.
Thibaut, Aurore, Sarah Wannez, Anne-Francoise Donneau, Camille Chatelle, Olivia Gosseries, Marie-Aurélie Bruno, and Steven Laureys. 2017. “Controlled Clinical Trial of Repeated Prefrontal tDCS in Patients with Chronic Minimally Conscious State.” *Brain Injury* 31 (4): 466–74.
Uchimura, Motoaki, Hironori Kumano, and Shigeru Kitazawa. 2024. “Neural Transformation from Retinotopic to Background-Centric Coordinates in the Macaque Precuneus.” *The Journal of Neuroscience : The Official Journal of the Society for Neuroscience* 44 (48). https://doi.org/10.1523/JNEUROSCI.0892-24.2024.
Uhrig, Lynn, Stanislas Dehaene, and Béchir Jarraya. 2014. “A Hierarchy of Responses to Auditory Regularities in the Macaque Brain.” *The Journal of Neuroscience: The Official Journal of the Society for Neuroscience* 34 (4): 1127–32.

Uhrig, Lynn, David Janssen, Stanislas Dehaene, and Béchir Jarraya. 2016. “Cerebral Responses to Local and Global Auditory Novelty under General Anesthesia.” *NeuroImage* 141 (November):326–40.
Uhrig, Lynn, Jacobo D. Sitt, Amaury Jacob, Jordy Tasserie, Pablo Barttfeld, Morgan Dupont, Stanislas Dehaene, and Bechir Jarraya. 2018. “Resting-State Dynamics as a Cortical Signature of Anesthesia in Monkeys.” *Anesthesiology* 129 (5): 942–58.
Vanduffel, W., D. Fize, J. B. Mandeville, K. Nelissen, P. Van Hecke, B. R. Rosen, R. B. Tootell, and G. A. Orban. 2001. “Visual Motion Processing Investigated Using Contrast Agent-Enhanced fMRI in Awake Behaving Monkeys.” *Neuron* 32 (4): 565–77.
Vincent, Justin L., Abraham Z. Snyder, Michael D. Fox, Benjamin J. Shannon, Jessica R. Andrews, Marcus E. Raichle, and Randy L. Buckner. 2006. “Coherent Spontaneous Activity Identifies a Hippocampal-Parietal Memory Network.” *Journal of Neurophysiology* 96 (6): 3517–31.
Virtanen, Pauli, Ralf Gommers, Travis E. Oliphant, Matt Haberland, Tyler Reddy, David Cournapeau, Evgeni Burovski, et al., 2020. “SciPy 1.0: Fundamental Algorithms for Scientific Computing in Python.” *Nature Methods* 17 (3): 261–72.
Vohryzek, Jakub, Gustavo Deco, Bruno Cessac, Morten L. Kringelbach, and Joana Cabral. 2020. “Ghost Attractors in Spontaneous Brain Activity: Recurrent Excursions Into Functionally-Relevant BOLD Phase-Locking States.” *Frontiers in Systems Neuroscience* 14 (April):20.
Wang, Xiaoyu, Yongkun Guo, Yunge Zhang, Jinju Li, Zhongqi Gao, Yingxin Li, Tianlin Zhou, Hui Zhang, Jianghong He, and Fengyu Cong. 2020. “Combined Behavioral and Mismatch Negativity Evidence for the Effects of Long-Lasting High-Definition tDCS in Disorders of Consciousness: A Pilot Study.” *Frontiers in Neuroscience* 14 (April):381.
Wan, Xiaoping, Yong Wang, Ye Zhang, and Weiqun Song. 2023. “A Comparison of the Neuromodulation Effects of Frontal and Parietal Transcranial Direct Current Stimulation on Disorders of Consciousness.” *Brain Sciences* 13 (9). https://doi.org/10.3390/brainsci13091295.
Wirth, Miranka, Rasha Abdel Rahman, Janina Kuenecke, Thomas Koenig, Helge Horn, Werner Sommer, and Thomas Dierks. 2011. “Effects of Transcranial Direct Current Stimulation (tDCS) on Behaviour and Electrophysiology of Language Production.” *Neuropsychologia* 49 (14): 3989–98.
Wu, Min, Yamei Yu, Lunjie Luo, Yuehao Wu, Jian Gao, Xiangming Ye, and Benyan Luo. 2019. “Efficiency of Repetitive Transcranial Direct Current Stimulation of the Dorsolateral Prefrontal Cortex in Disorders of Consciousness: A Randomized Sham-Controlled Study.” *Neural Plasticity* 2019 (June):7089543.
Xie, Hua, Javier Gonzalez-Castillo, Daniel A. Handwerker, Peter A. Bandettini, Vince D. Calhoun, Gang Chen, Eswar Damaraju, Xiangyu Liu, and Sunanda Mitra. 2019. “Time-Varying Whole-Brain Functional Network Connectivity Coupled to Task Engagement.” *Network Neuroscience (Cambridge, Mass.)* 3 (1): 49–66.
Yacoub, Essa, Mark D. Grier, Edward J. Auerbach, Russell L. Lagore, Noam Harel, Gregor Adriany, Anna Zilverstand, et al., 2020. “Ultra-High Field (10.5 T) Resting State fMRI in the Macaque.” *NeuroImage* 223 (December):117349.
Zhang, Chunyun, Shuai Han, Zean Li, Xinjun Wang, Chuanxiang Lv, Xiangyun Zou, Fulei Zhu, et al., 2022. “Multidimensional Assessment of Electroencephalography in the Neuromodulation of Disorders of Consciousness.” *Frontiers in Neuroscience* 16 (June):903703.
Zhang, Ye, Weiqun Song, Jubao Du, Su Huo, Guixiang Shan, and Ran Li. 2017. “Transcranial Direct Current Stimulation in Patients with Prolonged Disorders of Consciousness: Combined Behavioral and Event-Related Potential Evidence.” *Frontiers in Neurology* 8 (November):620.

Figures

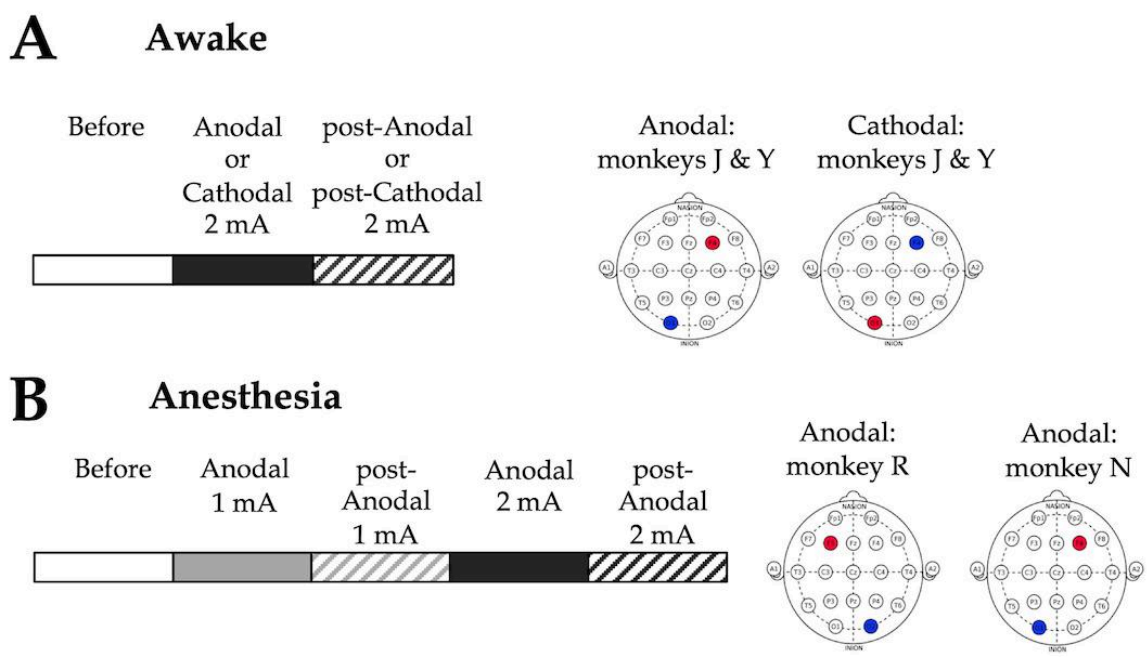

Figure 1. Schematic representation of the experimental designs and tDCS electrode montages employed in the study. A) Awake experiments. fMRI data were acquired before, during, and after 20 min of tDCS stimulation at 2 mA intensity. The anodal electrode (red) was either placed over the right prefrontal cortex (F4) and the cathodal electrode (blue) over the left occipital cortex (O1) ("anodal" montage), or a "reversed" montage was used, with the cathodal electrode over F4 and the anodal electrode over O1 ("cathodal" montage). **B)** Anesthesia experiments. fMRI data were recorded before, during, and after 20 min of consecutive 1 mA and 2 mA tDCS stimulation. An anodal electrode montage was employed, targeting the left or right prefrontal cortex (F4/O1 or F3/O2) depending on the animal and its anatomical constraints. Before: before stimulation. Anodal and post-Anodal: during and after anodal tDCS of the PFC. Cathodal and post-Cathodal: during and after cathodal tDCS of the PFC.

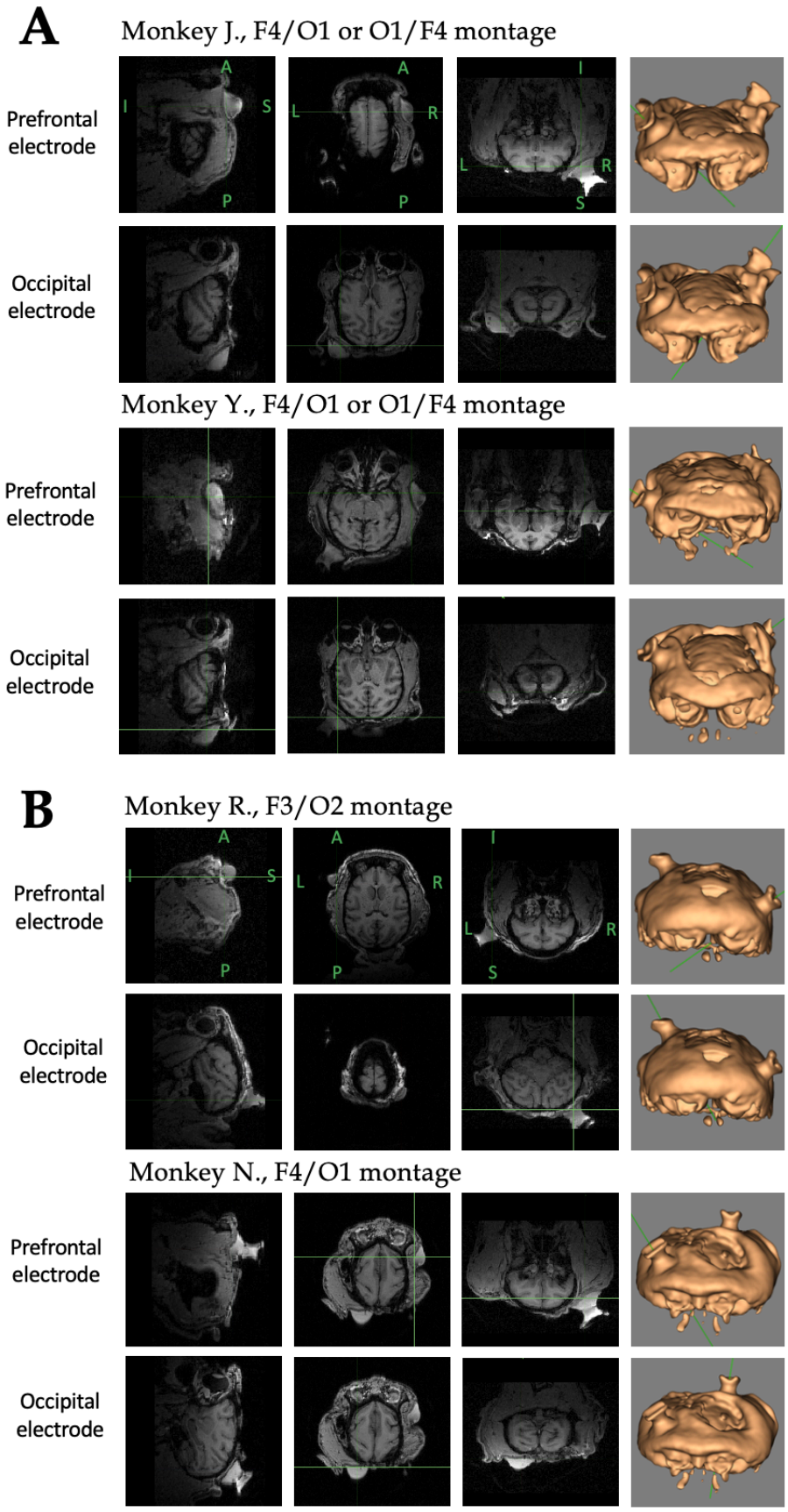
A
Monkey J., F4/O1 or O1/F4 montage
Prefrontal electrode
Occipital electrode
Monkey Y., F4/O1 or O1/F4 montage
Prefrontal electrode
Occipital electrode
B
Monkey R., F3/O2 montage
Prefrontal electrode
Occipital electrode
Monkey N., F4/O1 montage
Prefrontal electrode
Occipital electrode

Figure 1 - figure supplement 1. Structural images displaying electrode placements on the head of monkeys. A) Awake experiments. Representative sagittal, coronal and transverse MRI sections, and the corresponding skin reconstruction images showing the position of the prefrontal and the occipital electrodes on the head of monkeys J. and Y. **B)** Anesthesia experiments. Representative sagittal, coronal and transverse MRI sections, and the corresponding skin reconstruction images showing the position of the prefrontal and occipital electrodes over the occipital cortex on the head of monkeys R. and N.

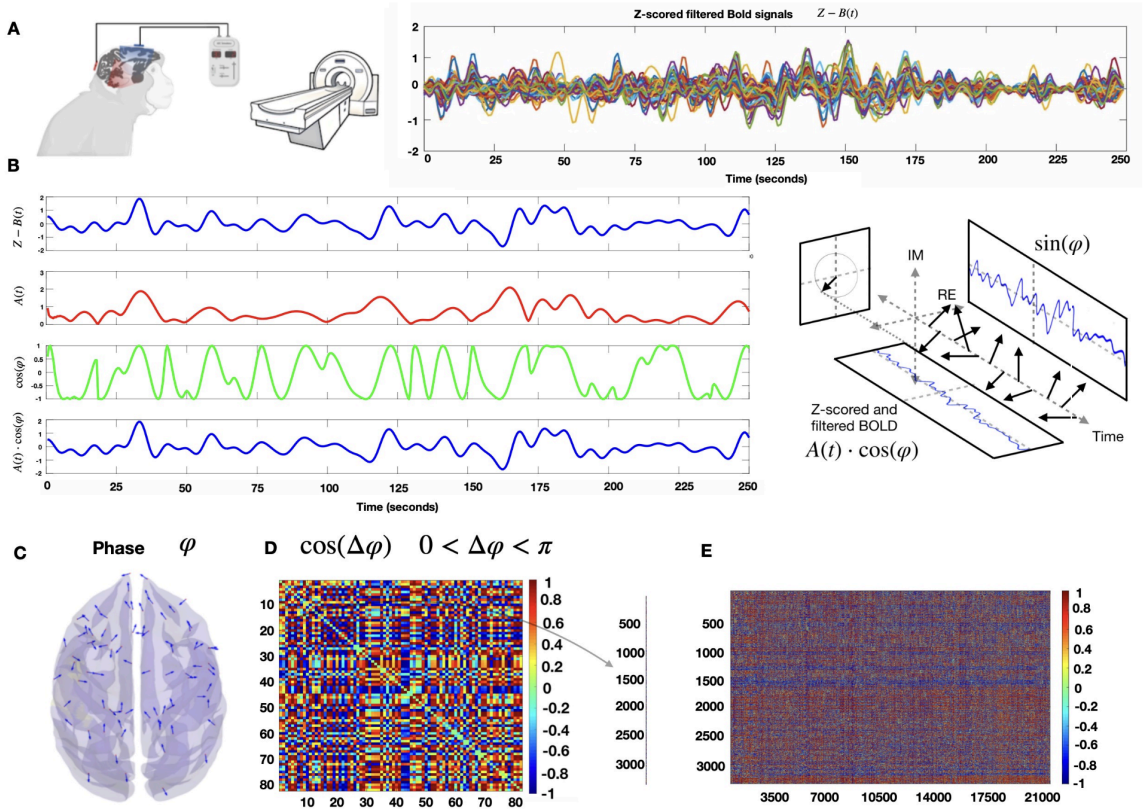

Figure 2. fMRI Phase Coherence analysis. A) Left) Animals were scanned before, during and after PFC tDCS stimulation in the awake state (two macaques) or under deep propofol anesthesia (two macaques). Right) Example of Z-scored filtered BOLD time series for one macaque. **B)** Hilbert transform of the z-scored BOLD signal of one ROI into its time-varying amplitude A(t) (red) and the real part of the phase φ (green). In blue, we recover the original z-scored BOLD signal as A(t)cos(φ). **C)** Example of the phase of the Hilbert transform for each brain region at one TR. **D)** Symmetric matrix of cosines of the phase differences between all pairs of brain regions. **E)** We extract the superior triangular half of the phase coherence matrix and vectorize it. All timepoints of the recordings from the different conditions are concatenated together.

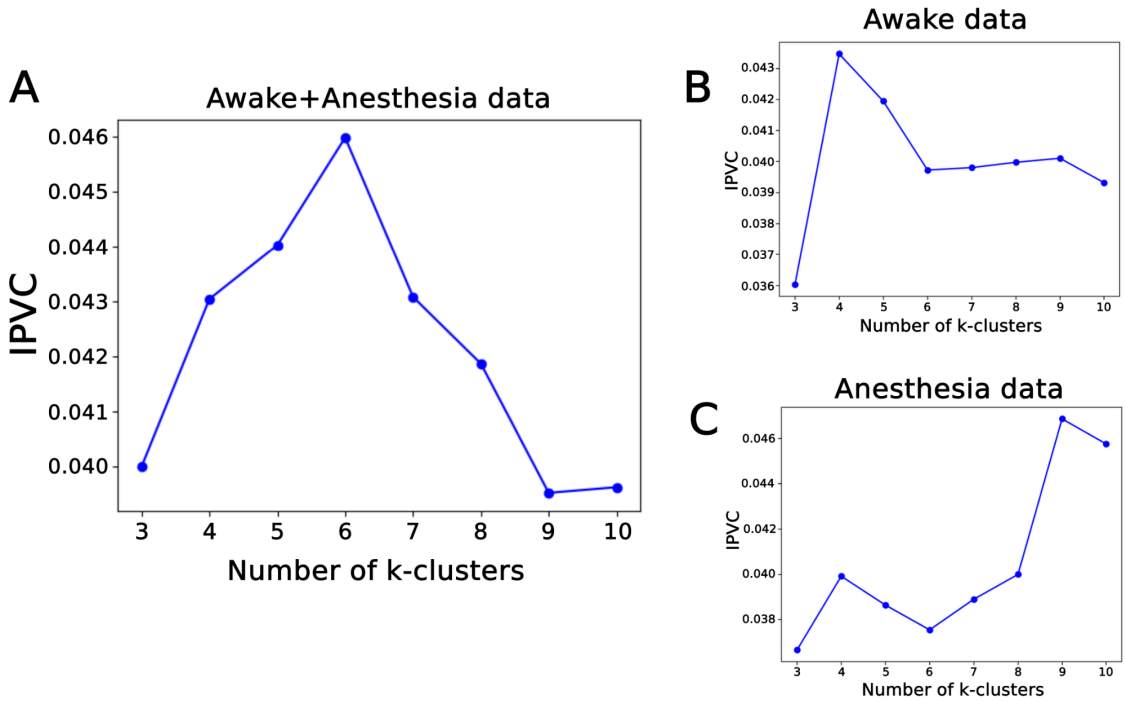

Figure 2 - figure supplement 1. Inter-pattern correlation variance (IPCV), a measure used to identify the optimal number of *k*-clusters (or brain patterns). A) IPCV obtained when awake and anesthesia datasets are considered together. **B)** IPCV obtained when only the awake dataset is considered. **C)** IPCV obtained with only the anesthesia dataset.

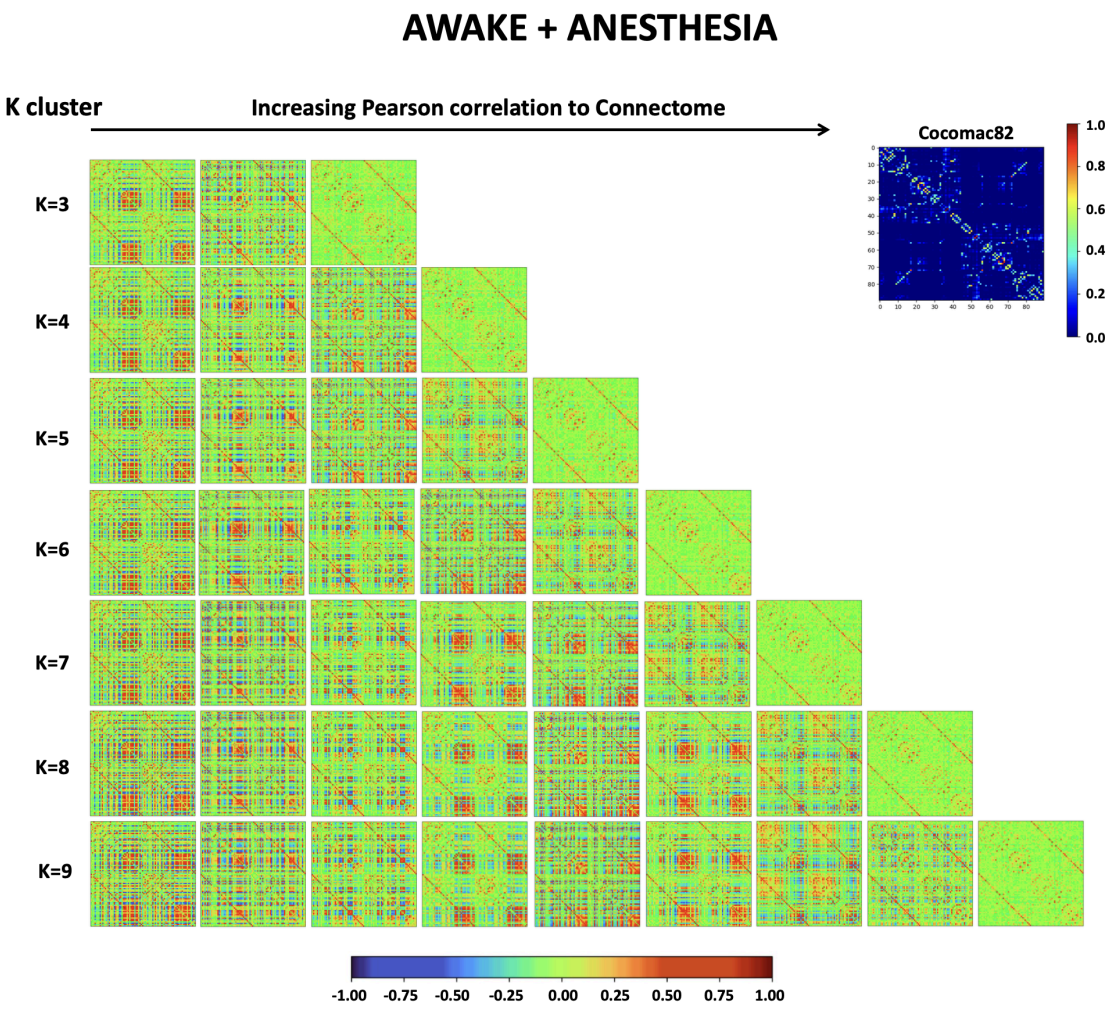

Figure 2 - figure supplement 2. Dynamical functional patterns from awake and anesthesia datasets. Matrix representation of the brain patterns for *k*=3 to 9 number of clusters in the k-means algorithm. The brain patterns were obtained by including all the awake (5 conditions) and anesthesia (5 conditions) data in the analysis and ordered from least (left) to most (right) similarity to the structural connectivity matrix.

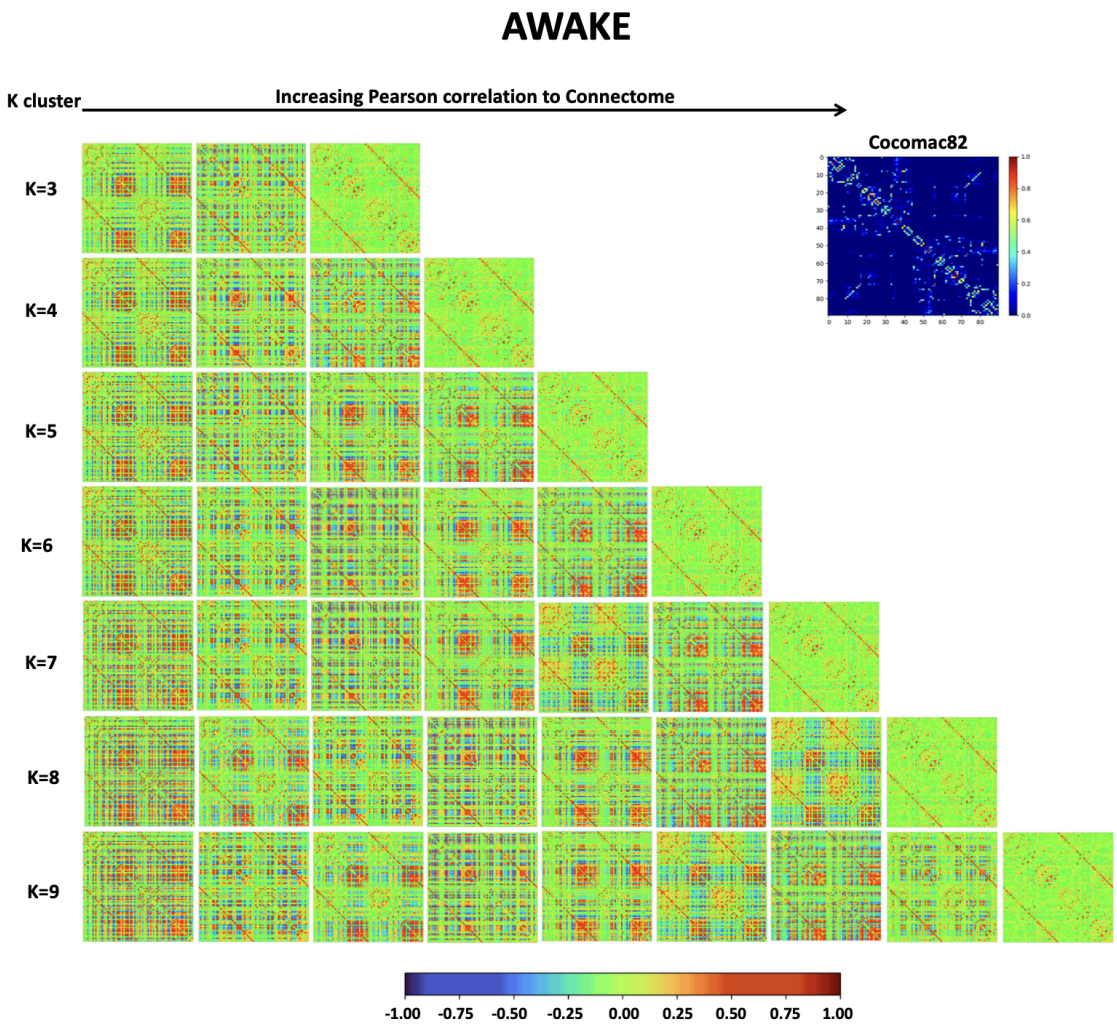

Figure 2 - figure supplement 3. Dynamical functional patterns from the awake dataset. Matrix representation of the brain patterns for *k*=3 to 9 number of clusters in the k-means algorithm. The brain patterns were obtained by including all five awake conditions and were ordered from least (left) to most (right) similarity to the structural connectivity matrix.

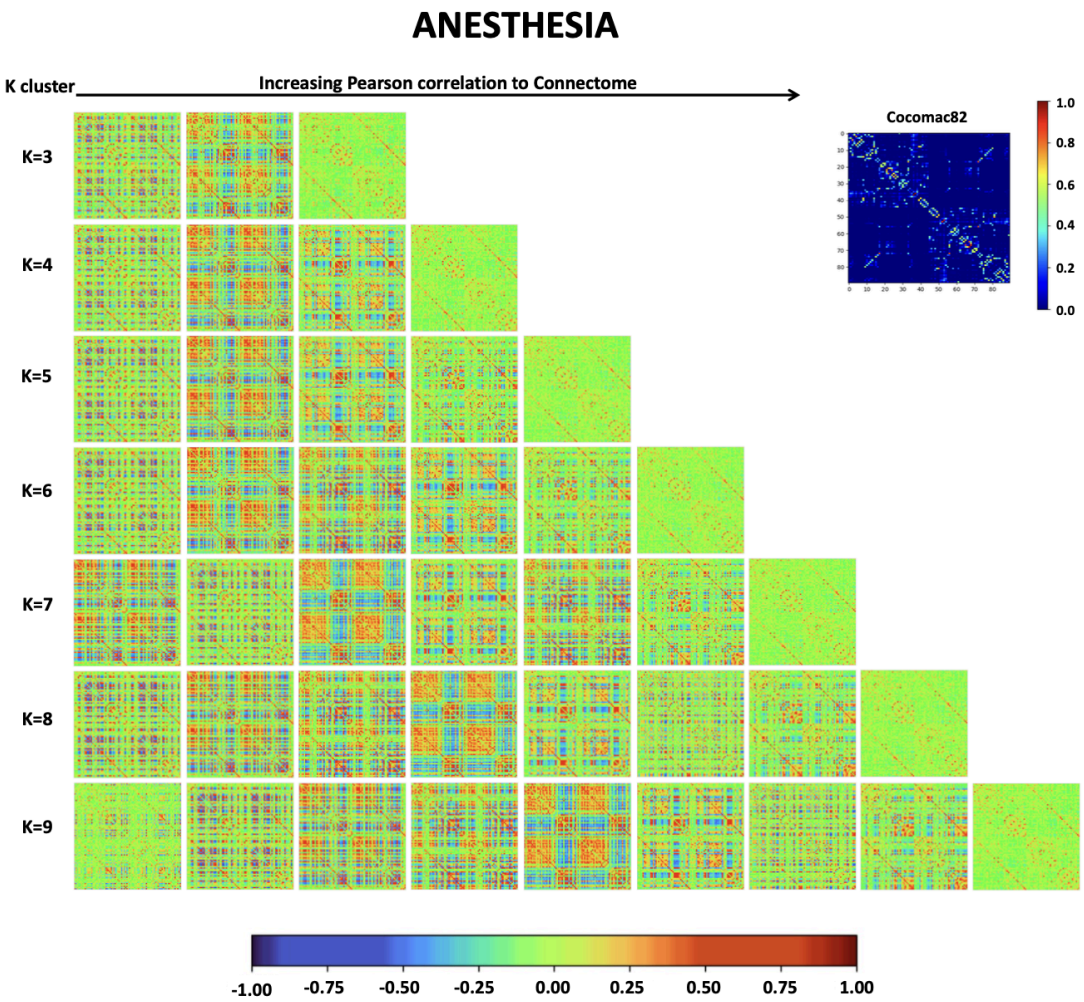

Figure 2 - figure supplement 4. Dynamical functional patterns from the anesthesia dataset. Matrix representation of the brain patterns for *k*=3 to 9 number of clusters in the k-means algorithm. The brain patterns were obtained by including all five anesthesia conditions and were ordered from least (left) to most (right) similarity to the structural connectivity matrix.

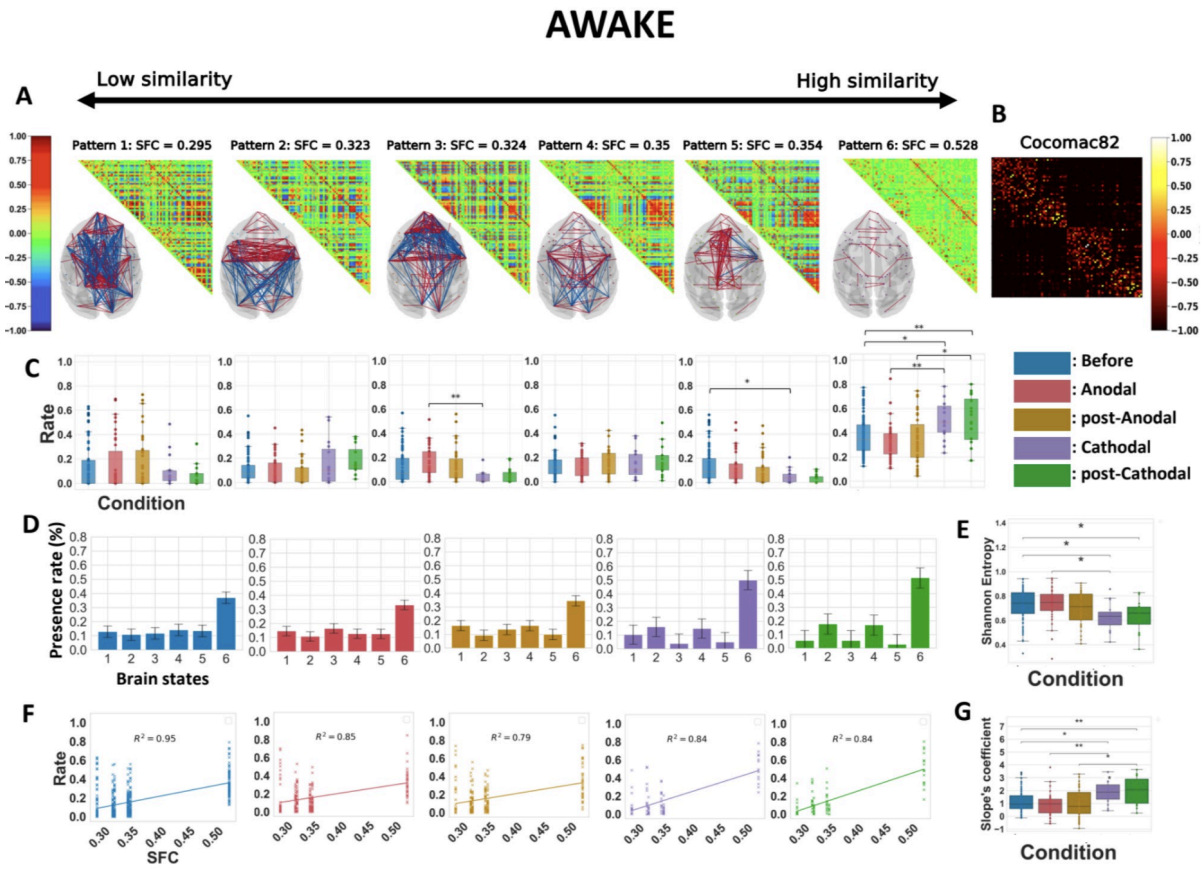

Figure 3. Cathodal but not anodal tDCS of the prefrontal cortex alters the repertoire of functional brain patterns, increases structure-function coupling and decreases Shannon Entropy in awake animals. A) Matrix representation of the brain patterns for *k* = 6, obtained by including all the five awake conditions. Brain coordination patterns are ranked from least (left) to highest (right) correlation to the structural connectivity matrix. Networks are plotted in anatomical space (transverse view), showing only values <-0.5 and >0.5. Red lines represent positive synchronizations between regions of interest, and blue lines represent negative ones. **B)** Macaque connectome in the CoCoMac82 parcellation. **C)** Rate of occurrence of each brain connectivity pattern across the five conditions. Boxplots show median occurrence rates with interquartile range and maximum-minimum values (whiskers). **D)** Barplots of the six brain states and their average presence rate over the different conditions. **E)** Normalized Shannon Entropy as a function of the conditions. **F)** Rates of occurrence of brain patterns as a function of their similarity in functional and structural connectivity (SFC) for the five conditions. Lines are calculated, per conditions, based on the best linear fit between the average presence rate of each pattern and their SFC. R^2, Spearman correlation. Crosses represent individuals' presence rates. **G)** Coefficient of the linearly regressed slope across conditions. Before: pre-stimulation, Anodal and post-Anodal: during and after anodal tDCS of the PFC (F4/O1 montage). Cathodal and post-Cathodal: during and after cathodal tDCS of the PFC (O1/F4 montage).

AWAKE

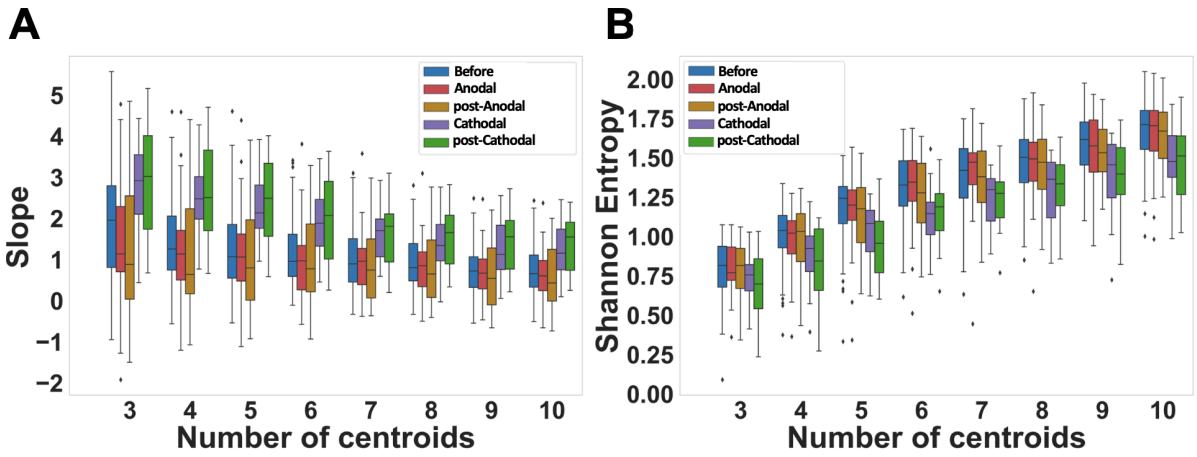

Figure 3 - figure supplement 1. Slope and Shannon entropy in the awake conditions. Slopes of the linear regression **(A)** and Shannon entropy **(B)** of the distribution of brain pattern occurrences computed for a number of clusters from 3 to 10 in the k-means algorithm. All five awake conditions were included in the analyses. The same relative differences were found for all values of *k* analyzed. In the cathodal prefrontal stimulation conditions, the slopes of the linear regression show a tendency towards anatomically driven dynamics, and the Shannon entropy is lower than in the pre-stimulation and anodal prefrontal stimulation conditions.

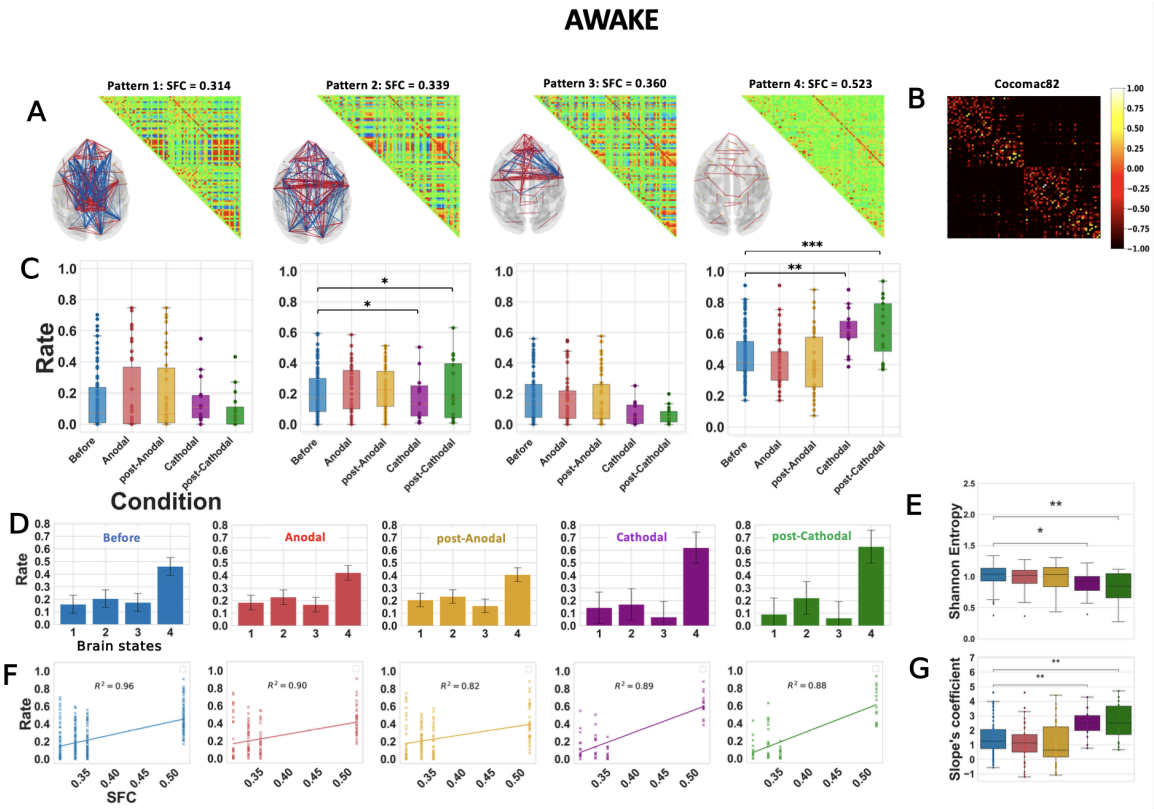

Figure 3 - figure supplement 2. Dynamical functional connectivity analysis of the awake dataset with *k* = 4 numbers of clusters. Similar analysis than in Figure 3 for *k*=4 considering all the five awake conditions. Before: before tDCS in the awake state. Anodal and post-Anodal: during and after anodal tDCS of the PFC (F4/O1 electrode montage) at an intensity of 2 mA. Cathodal and post-Cathodal: during and after cathodal tDCS of the PFC (O1/F4 montage) at an intensity of 2 mA.

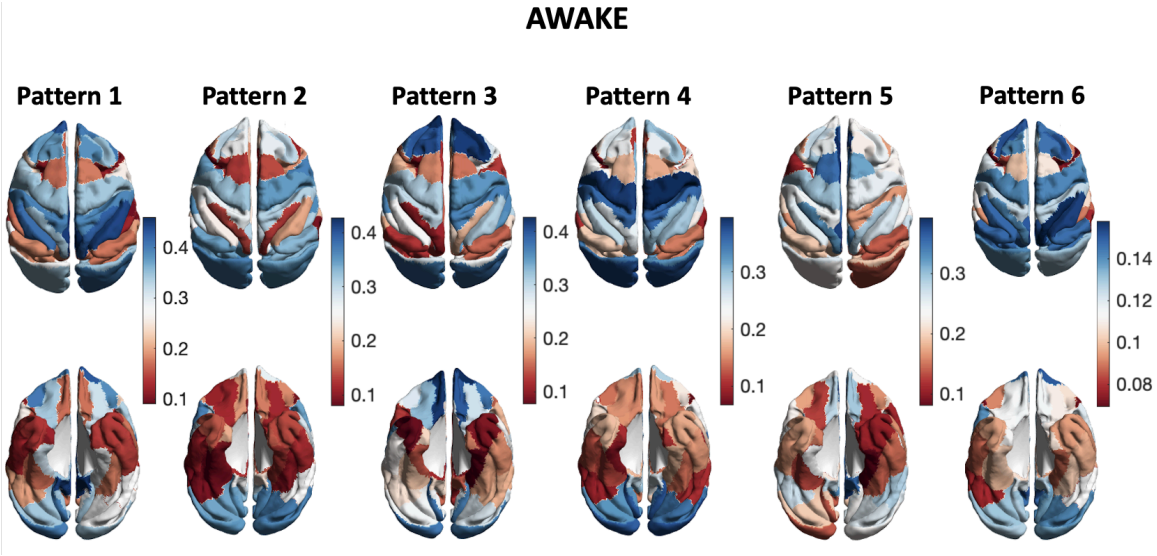

Figure 3 - figure supplement 3. Variance in inter-region phase coherences of brain patterns. Low values (red and light red) indicate that the distribution of synchronizations between a brain region and the rest of the brain has relatively low variance, while high values (blue and light blue) indicate relatively high variance. Are displayed both supra (top) and subdorsal (bottom) views for each brain pattern from the main figure, ordered similarly as previously: from left (1) to right (6) as their respective SFC increases.

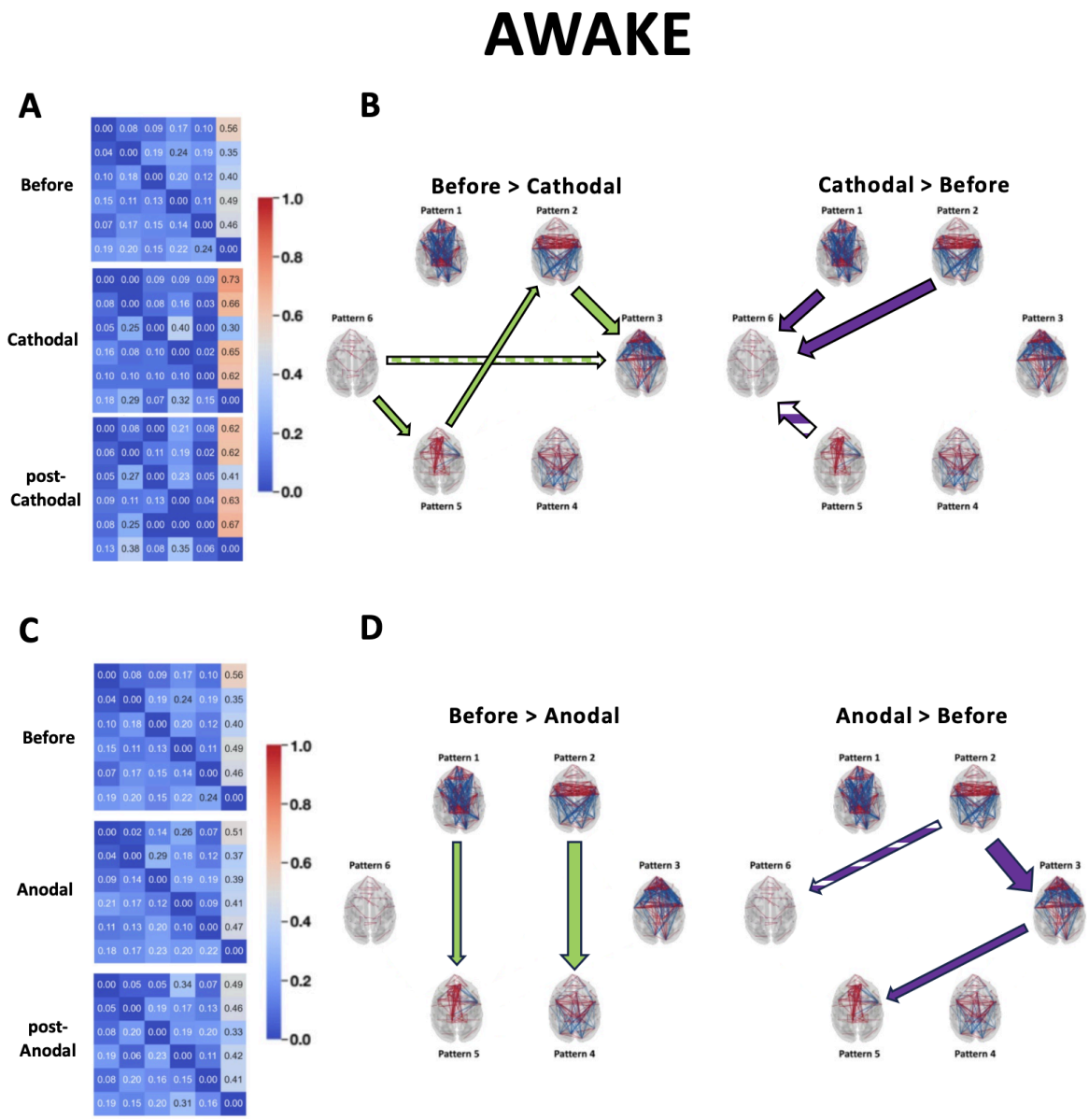

Figure 4. Transition probabilities and Markov chain analysis of the identified brain states during and after cathodal or anodal PFC stimulation in the awake state. A & C) Overall transition probabilities matrices pre-stimulation, during and after cathodal stimulation (A) or during and after anodal stimulation (C). **B & D)** Left panels: transition probabilities greater before stimulation than during stimulation (full green arrows) or post-stimulation (hashed green arrows). Right panels: transition probabilities greater during (full purple arrows) or after (hashed purple arrows) the stimulation than before. Arrow size indicates *p* value significance. Before: pre-stimulation. Cathodal and post-Cathodal: during and after cathodal tDCS of the PFC (O1/F4 montage). Anodal and post-Anodal: during and after anodal tDCS of the PFC (F4/O1 montage).

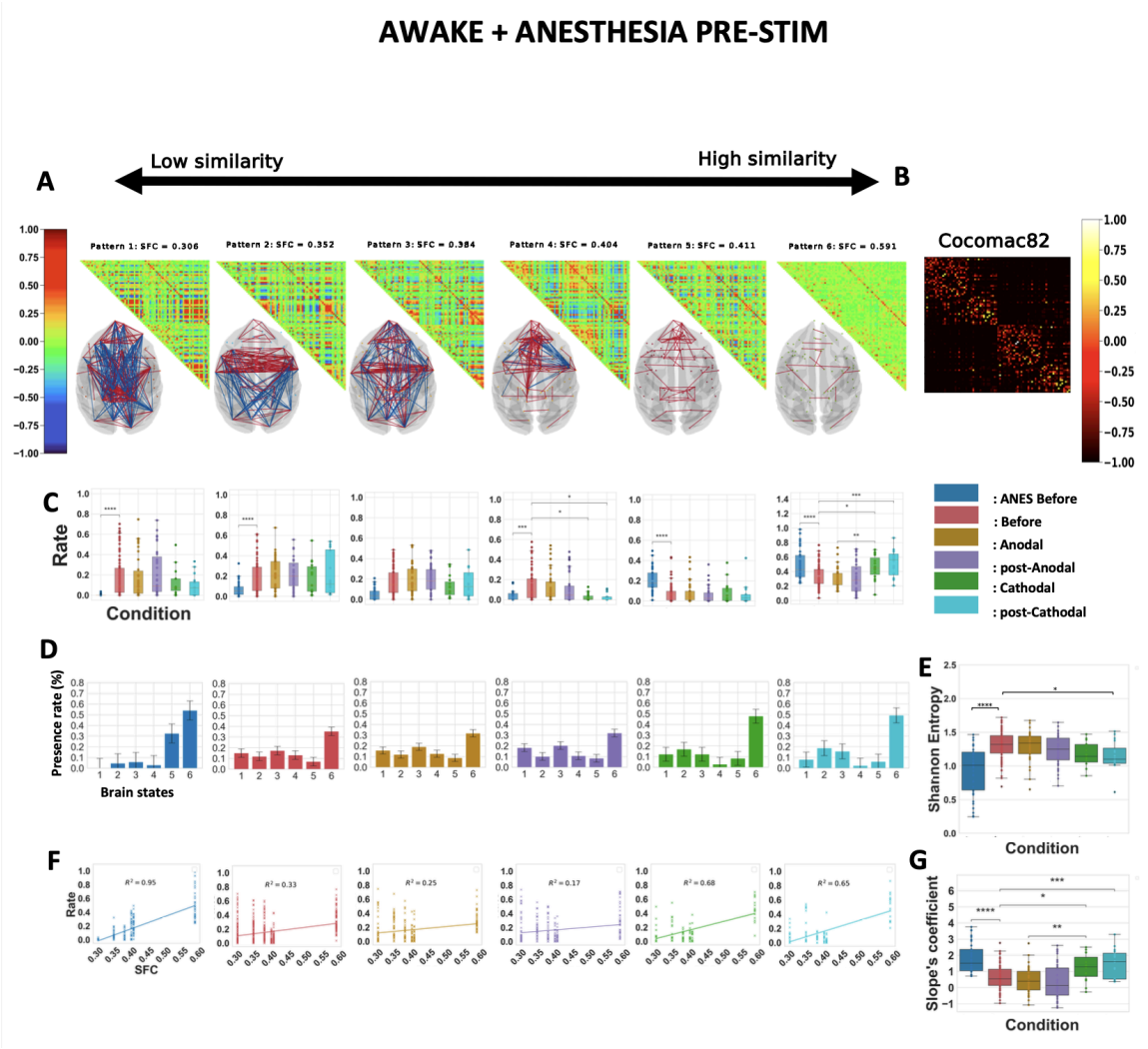

Figure 5. The polarity-dependent effects of prefrontal tDCS on awake brain dynamics resist contrasting with anesthetized dynamics. Similar analysis than in Figure 3 for *k*=6 considering all the five awake conditions plus the anesthesia pre-stimulation condition. ANES Before: before stimulation under anesthesia. Before: before stimulation in the awake state. Anodal and post-Anodal: during and after anodal tDCS of the PFC (F4/O1 montage) in the awake state. Cathodal and post-Cathodal: during and after cathodal tDCS of the PFC (O1/F4 montage) in the awake state.

AWAKE + ANESTHESIA PRE-STIM

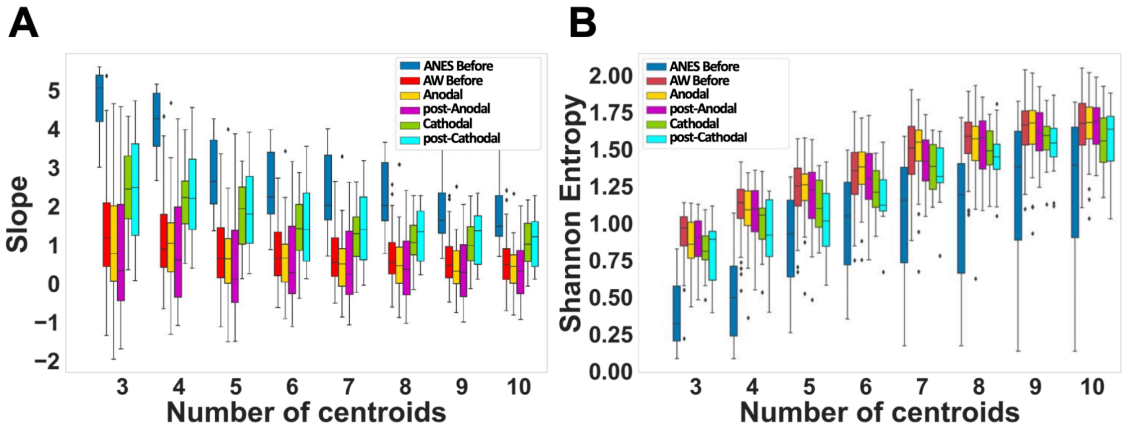

Figure 5 - figure supplement 1. Slope and Shannon entropy in awake conditions contrasted with anesthesia pre-stimulation condition. Slopes of the linear regression **(A)** and Shannon entropy **(B)** of the distribution of brain pattern occurrences computed for a number of clusters from 3 to 10 in the k-means algorithm. All five awake conditions plus the anesthesia pre-stimulation condition were included in the analyses. The same relative differences were found for all values of *k* analyzed. In the cathodal prefrontal stimulation conditions, the slopes of the linear regression are increased and tend to approach the values of the anesthesia pre-stimulation condition. Similarly, the Shannon entropy is lower in the cathodal stimulation conditions than in the pre-stimulation and anodal prefrontal stimulation conditions and moves towards the value of the anesthesia pre-stimulation condition.

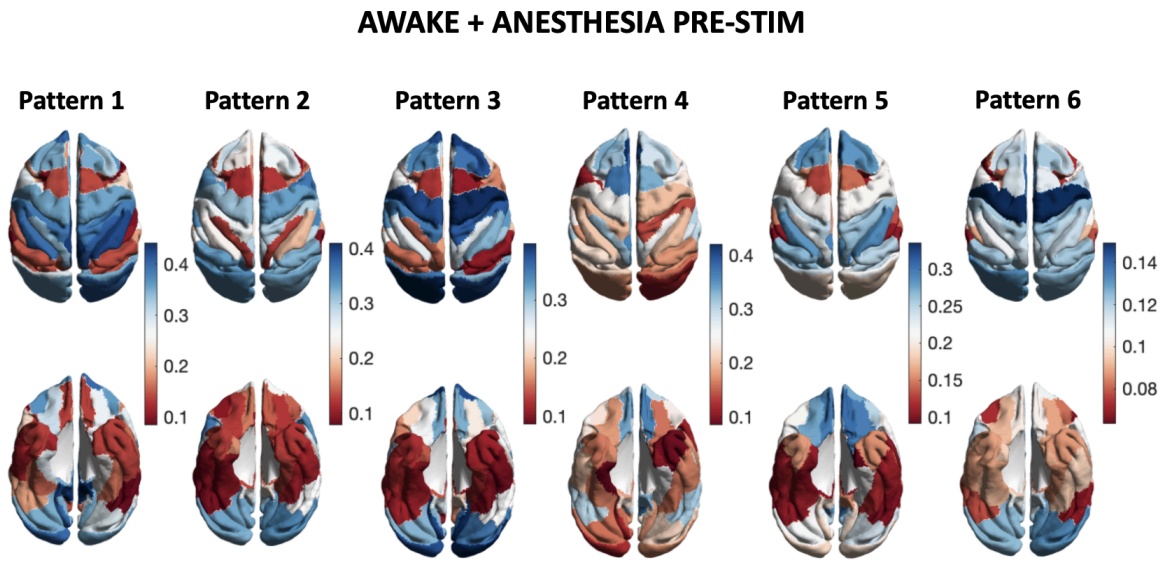

Figure 5 - figure supplement 2. Variance in inter-region phase coherences of brain patterns. Low values (red and light red) indicate that the distribution of synchronizations between a brain region and the rest of the brain has relatively low variance, while high values (blue and light blue) indicate relatively high variance. Are displayed both supra (top) and subdorsal (bottom) views for each brain pattern from the main figure, ordered similarly as previously: from left (1) to right (6) as their respective SFC increases.

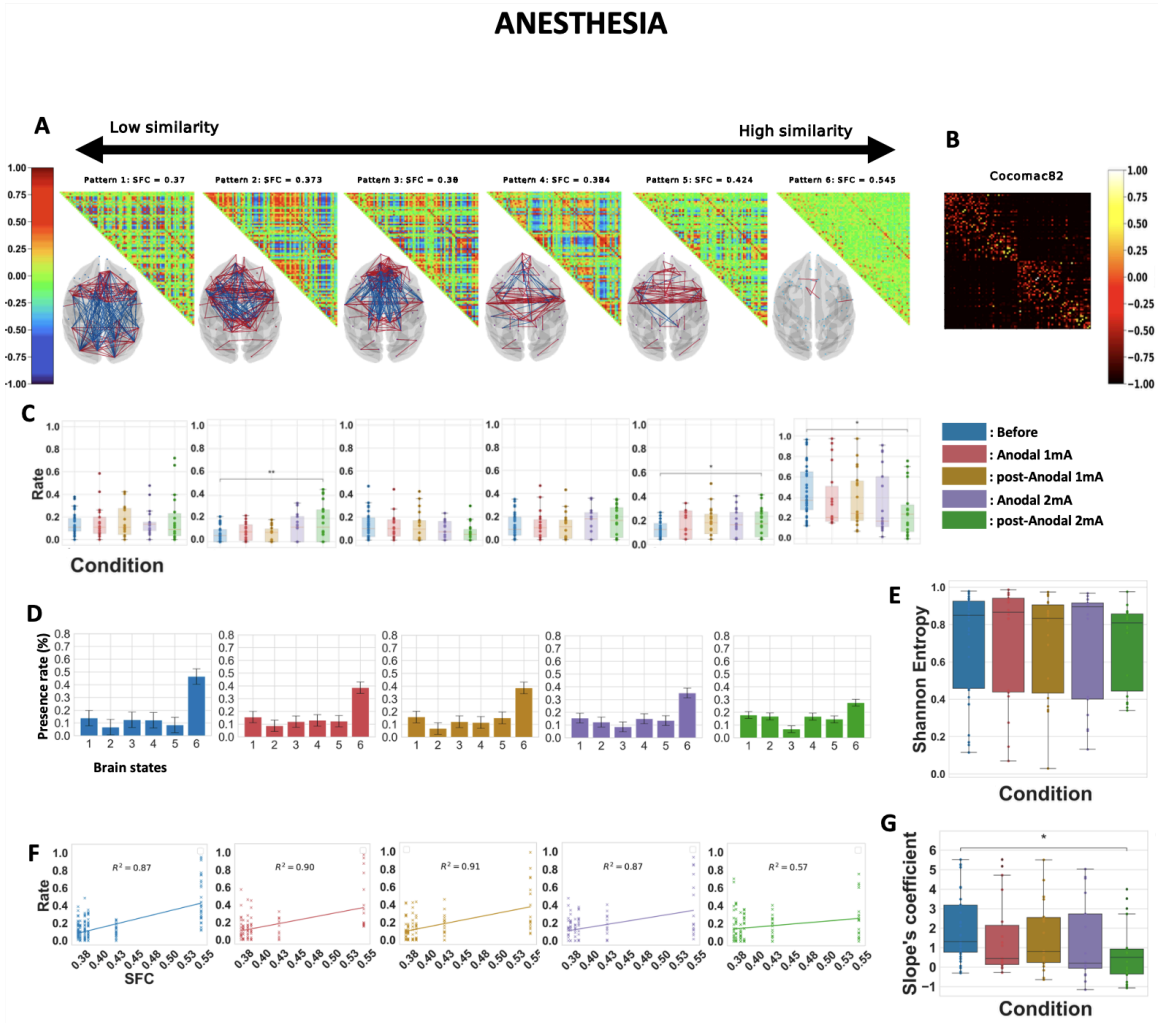

Figure 6. Anodal 2 mA tDCS of the prefrontal cortex modifies cortical brain dynamics and reduces structure-function coupling in anesthetized animals. Similar analysis than in Figures 3 and 5 for *k*=6 considering all the five anesthesia conditions. Before: before stimulation. Anodal 1 mA and post-Anodal 1 mA: during and after anodal tDCS of the PFC (F4/O1 or F3/O2) delivered at an intensity of 1 mA. Anodal 2 mA and post-Anodal 2 mA: during and after anodal tDCS of the PFC (F4/O1 or F3/O2 montage) delivered at an intensity of 2 mA.

ANESTHESIA

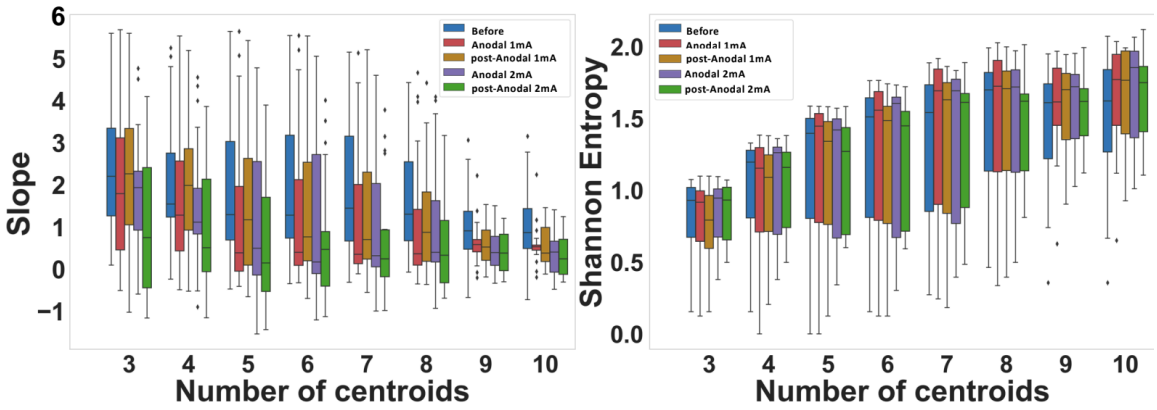

Figure 6 - figure supplement 1. Slope and Shannon entropy in anesthesia conditions. Slopes of the linear regression **(A)** and Shannon entropy **(B)** of the distribution of brain patterns occurrences computed for a number of clusters from 3 to 10 in the k-means algorithm. All five anesthesia conditions were included in the analyses. The same relative differences were found for all values of *k* analyzed. In the 2 mA stimulation conditions, the slopes of the linear regression are decreased compared to the pre-stimulation condition.

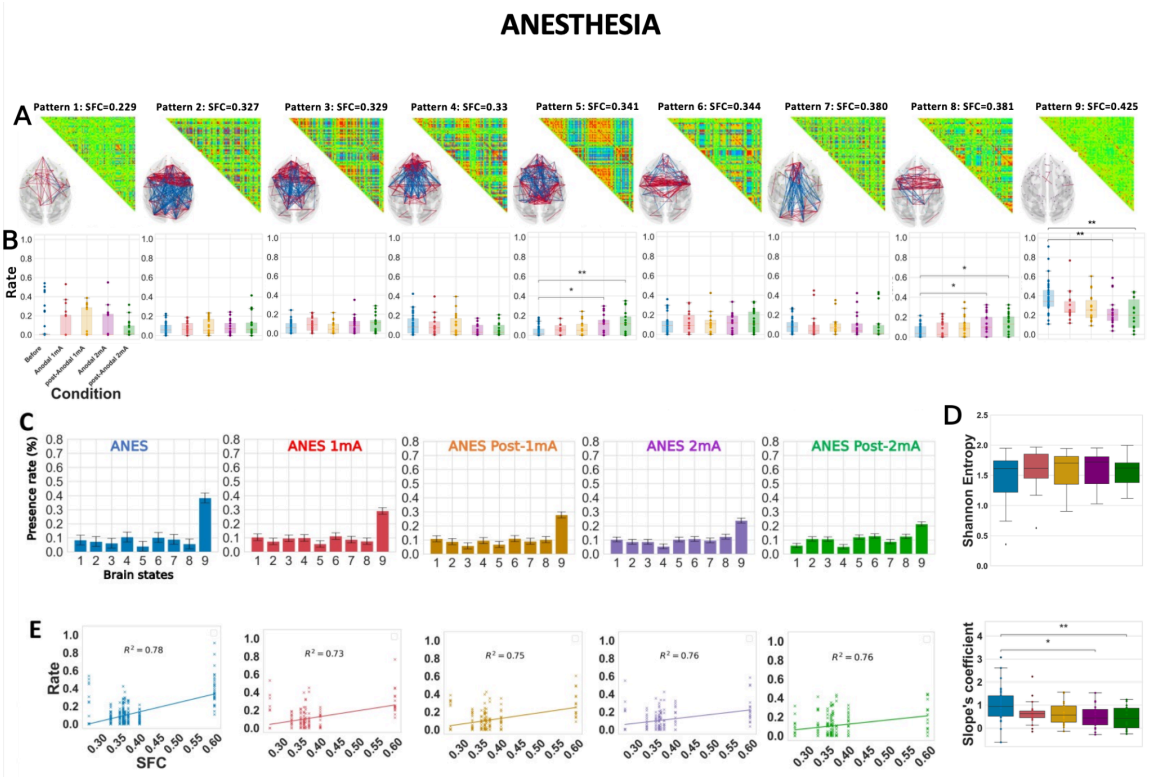

Figure 6 - figure supplement 2. Dynamical functional connectivity analysis of the anesthesia dataset with *k* = 9 numbers of clusters. Similar analysis than in Figure 6 for *k*=9 considering all the five anesthesia conditions. Before: before stimulation, under anesthesia. Anodal 1 mA, post-Anodal 1 mA: during and after anodal tDCS of the PFC at 1 mA intensity. Anodal 2 mA and post-Anodal 2 mA: during and after anodal tDCS of the PFC at 2 mA intensity.

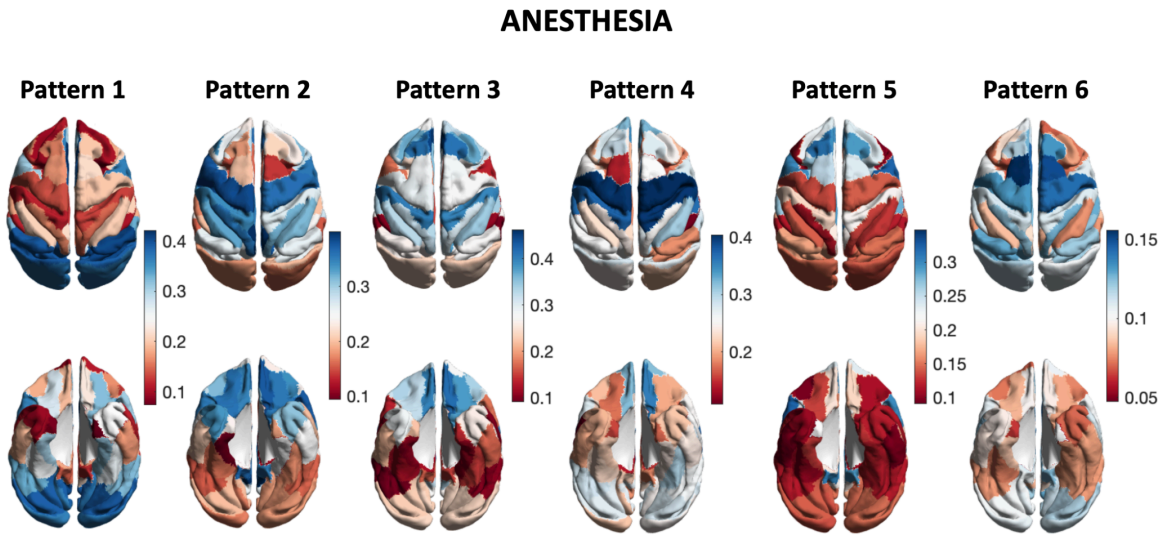

Figure 6 - figure supplement 3. Variance in inter-region phase coherences of brain patterns. Low values (red and light red) indicate that the distribution of synchronizations between a brain region and the rest of the brain has relatively low variance, while high values (blue and light blue) indicate relatively high variance. Are displayed both supra (top) and subdorsal (bottom) views for each brain pattern from the main figure, ordered similarly as previously: from left (1) to right (6) as their respective SFC increases.

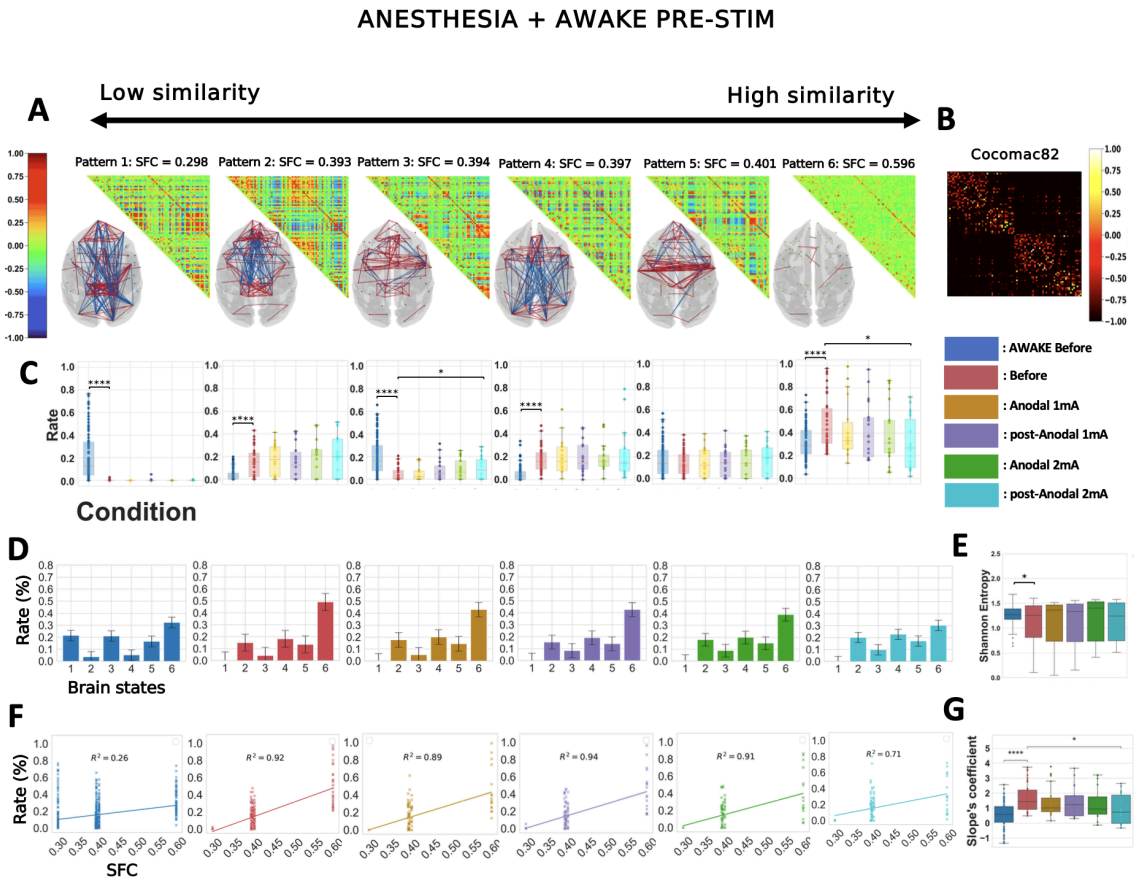

Figure 7. The effects of 2 mA anodal prefrontal tDCS on anesthesia brain dynamics resist contrasting with awake dynamics. Similar analysis than in Figure 6 for *k*=6 considering all the five anesthesia conditions plus the awake pre-stimulation condition. Awake before: before stimulation in the awake state. Before: before stimulation, under anesthesia. Anodal 1 mA, Post-anodal 1 mA: during and after anodal tDCS of the PFC at 1 mA intensity. Anodal 2 mA and post-Anodal 2 mA: during and after anodal tDCS of the PFC at 2 mA intensity.

ANESTHESIA + AWAKE PRE-STIM

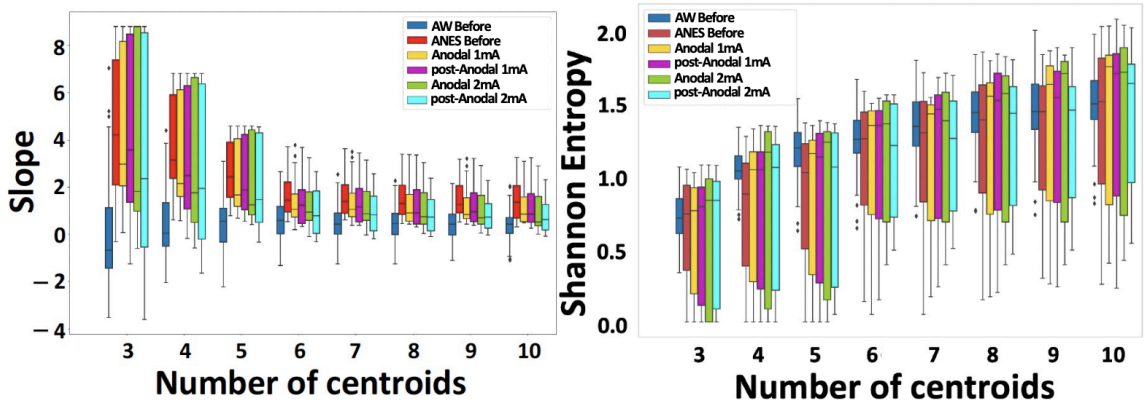

Figure 7 - figure supplement 1. Slope and shannon Entropy in anesthesia conditions contrasted with awake pre-stimulation condition. Slopes of the linear regression **(A)** and Shannon Entropy **(B)** of the distribution of brain pattern occurrences computed for a number of clusters from 3 to 10 in the k-means algorithm. All five anesthesia conditions plus the awake pre-stimulation condition were included in the analyses. The same relative differences were found for all values of k analyzed. In the 2 mA stimulation conditions, the slopes of the linear regression are decreased and tend to approach the values of the awake pre-stimulation condition.

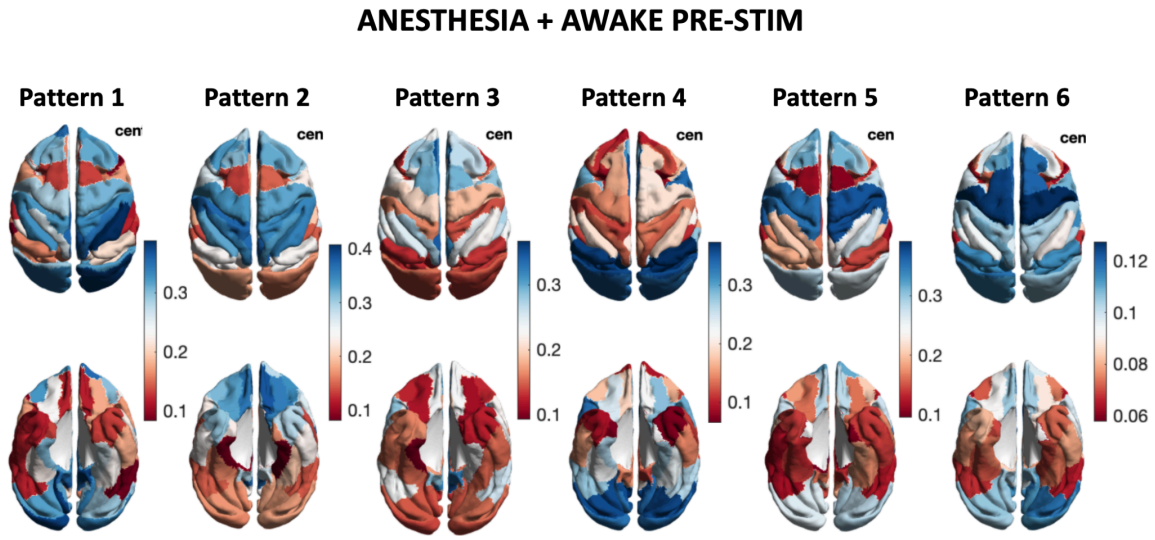

Figure 7 - figure supplement 2. Variance in inter-region phase coherences of brain patterns. Low values (red and light red) indicate that the distribution of synchronizations between a brain region and the rest of the brain has relatively low variance, while high values (blue and light blue) indicate relatively high variance. Are displayed both supra (top) and subdorsal (bottom) views for each brain pattern from the main figure, ordered similarly as previously: from left (1) to right (6) as their respective SFC increases.

Tables

Table 1. Number of fMRI runs acquired in each condition for each monkey, in awake and deeply sedated states.

Awake state	**Monkey J**	**Monkey Y**
Before tDCS	76	60
Anodal 2 mA tDCS	32	24
Post-anodal 2 mA tDCS	32	24
Cathodal 2 mA tDCS	12	8
Post-cathodal 2 mA tDCS	12	8

Anesthetized state	**Monkey R**	**Monkey N**
Before tDCS	32	8
Anodal 1 mA tDCS	16	8
Post-anodal 1 mA tDCS	16	8
Anodal 2 mA tDCS	16	8
Post-anodal 2 mA tDCS	16	8

Table 2. Percentage of eye fixation during tDCS fMRI experiments in the awake state.

Condition	Animal	Fixation (%)
Before tDCS	Monkey J	99 +/- 2
	Monkey Y	98 +/- 4
Anodal 2 mA tDCS	Monkey J	99 +/- 3
	Monkey Y	99 +/- 2
Post-anodal 2 mA tDCS	Monkey J	98 +/- 3
	Monkey Y	98 +/- 3
Cathodal 2 mA tDCS	Monkey J	99 +/- 1
	Monkey Y	100 +/- 1
Post-cathodal 2 mA tDCS	Monkey J	100 +/- 1
	Monkey Y	100 +/- 1

Table 3. Physiological data during tDCS fMRI experiments under deep propofol anesthesia. Physiological parameters under deep propofol anesthesia and different tDCS stimulation conditions: heart rate; oxygen saturation (SpO2); systolic blood pressure (SAP); diastolic blood pressure (DAP); respiration rate; end-tidal CO2. *: statistically significant difference compared to pre-stimulation, at $p < 0.05$ with Bonferroni correction. In brackets, the standard deviation.

Condition	Heart rate	SpO2	SAP	DAP	Respiration rate	$EtCO_2$
Before tDCS	127 (10)	97 (3)	116 (11)	60 (7)	20 (2)	40 (1)
Anodal 1 mA tDCS	123 (8)	98 (1)	118 (9)	60 (4)	19 (2)	40 (1)
Post-anodal 1 mA tDCS	**120 (7)***	98 (1)	118 (9)	61 (4)	19 (2)	39 (1)
Anodal 2 mA tDCS	**120 (7)***	98 (1)	120 (6)	63 (3)	19 (2)	39 (1)
Post-anodal 2 mA tDCS	123 (4)	98 (1)	**123 (4)***	**65 (3)***	19 (2)	40 (1)

A one-way ANOVA revealed that there was a statistically significant difference in mean heart rate between at least two conditions ($F(4, 111) = [3.64]$, $p = [0.008]$). The Bonferonni test for multiple comparisons found that the mean value of heart rate in the post-stimulation 1 mA and stimulation 2 mA conditions was significantly lower compared to pre-stimulation (($p = 0.024$, 95% C.I. = [0.52,13.05]) and ($p = 0.021$, 95% C.I. = [0.62,13.15]), respectively). There was also a statistically significant difference in mean systolic and diastolic blood pressure between at least two conditions (($F(4, 131) = [2.97]$, $p = [0.022]$) and ($F(4, 130) = [3.07]$, $p = 0.018$]), respectively). The Bonferonni test showed that the mean systolic and diastolic blood pressures for the 2 mA post-stimulation condition were significantly higher compared to the pre-stimulation condition (($p = 0.017$, 95% C.I. = [-13.51,-0.77]) and ($p = 0.033$, 95% C.I. = [-8.36,-0.20]), respectively).

Table 4. Statistical analyses.

Table 4A. Awake experiments

T-test independent sample, Bonferroni correction, comparing occurrence of brain states'

Brain state #	***Compared conditions***	***Mean (SD)***	***df***	***t-value***	***Adjusted p-value***
6	Cathodal	0.50 (0.15)	95	3.0	0.013
	Before	0.37 (0.15)			
6	post-Cathodal	0.51 (0.18)	96	3.3	0.0052
	Before	0.37 (0.15)			
6	Anodal	0.33 (0.14)	51	3.7	0.002
	Cathodal	0.50 (0.15)			
6	post-Anodal	0.34 (0.18)	53	3.0	0.016
	post-Cathodal	0.51 (0.18)			
5	post-Cathodal	0.028 (0.035)	96	3.0	0.012
	Before	0.14 (0.14)			
3	Anodal	0.16 (0.12)	51	3.7	0.0022
	Cathodal	0.038 (0.046)			

Three-ways ANOVA type II

Brain state #		***Sum of Squares***	***df***	***f-value***	***p-value***
6	C(Montage)	1.8e-14	2	3.7e-13	0.99
	C(Time)	**4.2**	**2**	**84**	**<0.001**
	C(Animal)	NaN	1	NaN	NaN
	C(Montage):C(Time)	**1.1**	**4**	**11**	**<0.001**
	C(Montage):C(Animal)	6.9e-4	2	0.014	0.91
	C(Time):C(Animal)	4.6e-5	2	9.2e-4	0.97
	C(Montage):C(Time):C(Animal)	**0.99**	**4**	**9.9**	**<0.001**
	Residual	4.5	180	NaN	
5	C(Montage)	1.7e-14	2	6.5e-13	0.99
	C(Time)	0.023	2	0.87	0.35
	C(Animal)	NaN	1	NaN	NaN
	C(Montage):C(Time)	**0.17**	**4**	**3.2**	**0.04**
	C(Montage):C(Animal)	**0.24**	**2**	**9.1**	**0.0029**
	C(Time):C(Animal)	4.3e-4	2	0.016	0.89
	C(Montage):C(Time):C(Animal)	0.14	4	2.8	0.066
	Residual	2.3	180	NaN	

	C(Montage)	2.7e-14	2	1.2e-12	0.99
	C(Time)	**0.26**	**2**	**12**	**<0.001**
	C(Animal)	NaN	1	NaN	NaN
	C(Montage):C(Time)	**0.27**	**4**	**6.1**	**0.0026**
	C(Montage):C(Animal)	0.039	2	1.8	0.18
	C(Time):C(Animal)	0.028	2	1.3	0.25
	C(Montage):C(Time):C(Animal)	0.12	4	2.6	0.07
3	Residual	1.9	180	NaN	

T-test independent sample, Bonferroni correction, comparing non-normalized Shannon Entropies

Compared conditions	***Mean (SD)***	***df***	***t-value***	***Adjusted p-value***
Cathodal	1.1 (0.20)			
Before	1.3 (0.23)	95	2.5	0.037
post-Cathodal	1.1 (0.22)			
Before	1.3 (0.23)	96	2.5	0.04
Anodal	1.3 (0.23)			
Cathodal	1.1 (0.20)	51	2.6	0.035

T-test independent sample, Bonferroni correction, comparing slopes' coefficients

Compared conditions	***Mean (SD)***	***df***	***t-value***	***Adjusted p-value***
Cathodal	1.9 (0.85)			
Before	1.0 (0.86)	95	2.9	0.018
post-Cathodal	2.0 (1.0)			
Before	1.0 (0.86)	96	3.4	0.0043
Anodal	1.0 (0.80)			
Cathodal	1.9 (0.85)	51	3.5	0.0038
post-Cathodal	2.0 (1.0)			
post-Anodal	1.0 (1.1)	53	3.0	0.014

Table 4B. Markov transition

T-test independent* samples with Bonferroni correction

Transition	***Compared conditions***	***Mean (SD)***	***df***	***t-value***	***Adjusted p-value***
2 → 4	Before	0.24 (0.18)	118	2.4	0.019
	Anodal	0.16 (0.23)			
3 → 5	Before	0.056 (0.13)		3.1	0.0074
	Anodal	0.15 (0.19)			
2 → 6	Before	0.34 (0.05)		4.7	0.0018
	post-Anodal	0.47 (0.24)			
6 → 5	Before	0.24 (0.11)	95	2.7	0.043
	Cathodal	0.15 (0.16)			
5 → 2	Before	0.17 (0.11)		2.2	0.029
	Cathodal	0.10 (0.12)			
2 → 3	Before	0.19 (0.17)		2.4	0.01
	Cathodal	0.08 (0.11)			
1 → 6	Before	0.56 (0.11)		5.7	0.002
	Cathodal	0.73 (0.08)			
2 → 6	Before	0.35 (0.18)		3.6	<0.001
	Cathodal	0.66 (0.32)			
6 → 3	Before	0.15 (0.10)	96	2.3	0.024
	post-Cathodal	0.08 (0.11)			
5 → 6	Before	0.46 (0.15)		4.8	<0.001
	post-Cathodal	0.67 (0.23)			

*: Certain transitions, including transitions from brain states 4 and 5 to brain state 6, were affected both during and after cathodal stimulation. Such transitions were favored during and post-stimulation but did not pass the bootstrap and/or the ANOVA tests.

Table 4C. Awake conditions + anesthesia pre-stimulation condition

T-test independent samples with Bonferroni correction

Brain state #	***Compared conditions***	***Mean (SD)***	***df***	***t-value***	***Adjusted p-value***
	Cathodal	0.027 (0.036)			
	Before	0.13 (0.15)	95	2.6	0.019
	post-Cathodal	0.023 (0.037)			
4	Before	0.13 (0.15)	96	2.8	0.011
	Anes Before	0.54 (0.23)			
	Before	0.35 (0.14)	114	5.2	<0.001
	Cathodal	0.47 (0.16)			
	Before	0.35 (0.14)	95	2.9	0.021
	post-Cathodal	0.48 (0.17)			
	Before	0.35 (0.14)	96	3.1	0.0098
	Cathodal	0.47 (0.16)			
6	Anodal	0.32 (0.14)	51	3.4	0.0049

Two-ways* ANOVA type II

Brain state #		***Sum of Squares***	***df***	***f-value***	***p-value***
	C(Montage)	**0.27**	**2**	**7.5**	**0.0065**
	C(Time)	0.094	2	2.7	0.10
	C(Montage):C(Time)	**0.37**	**4**	**5.3**	**0.0056**
4	Residual	3.9	219	NaN	
	C(Montage)	**4.3**	**2**	**61.0**	**<0.001**
	C(Time)	**0.63**	**2**	**8.9**	**0.0032**
	C(Montage):C(Time)	**1.1**	**4**	**7.9**	**<0.001**
6	Residual	7.7	219	NaN	

*: Due to the monkeys from the anesthesia datasets being different animals than those from the awake dataset, including the animal specialness as independent variable resulted in completely NaN 3-ways ANOVA results. Hence, we removed said variable to at least verify the effect of montage type and time.

T-test independent sample, Bonferroni correction, comparing normalized Shannon Entropies

Compared conditions	***Mean (SD)***	***df***	***t-value***	***Adjusted p-value***
Before	0.73 (0.12)			
post-Cathodal	0.65 (0.098)	95	2.3	0.049
Before	0.73 (0.12)			
Anes Before	0.51 (0.20)	114	7.0	<0.001

T-test independent sample, Bonferroni correction, comparing slopes' coefficients

Compared conditions	***Mean (SD)***	***df***	***t-value***	***Adjusted p-value***
Cathodal	1.3 (0.80)			
Before	0.69 (0.72)	95	2.8	0.014
post-Cathodal	1.3 (0.85)			
Before	0.69 (0.72)	96	3.0	0.003
Cathodal	1.3 (0.80)			
Anodal	0.55 (0.74)	51	3.0	0.0072
post-Cathodal	1.3 (0.85)			
post-Anodal	0.55 (0.74)	53	2.6	0.023

Table 4D. Experiments under anesthesia

T-test independent samples with Bonferroni correction

Brain state #	***Compared conditions***	***Mean (SD)***	***df***	***t-value***	***Adjusted p-value***
2	Before	0.067 (0.070)	103	3.1	0.0035
	post-Anodal 2mA	0.17 (0.17)			
5	Before	0.084 (0.069)		2.2	0.030
	post-Anodal 2mA	0.15 (0.12)			
6	Before	0.46 (0.25)		3.1	<0.001
	post-Anodal 2mA	0.27 (0.24)			

Three-ways ANOVA type II

Brain state #		***Sum of Squares***	***df***	***f-value***	***p-value***
2	C(Montage)	-6.7e-17	2	-6.3e-15	1.0
	C(Time)	1.7e-15	2	1.7e13	1.0
	C(Animal)	**0.45**	**1**	**88**	**<0.001**
	C(Montage):C(Time)	**0.18**	**4**	**8.9**	**<0.001**
	C(Montage):C(Animal)	1.9e-17	2	1.8e-15	1.0
	C(Time):C(Animal)	-4.9e-18	2	-4.7-16	1.0
	C(Montage):C(Time):C(Animal)	**0.083**	**4**	**4.0**	**0.0047**
	Residual	0.49	95	NaN	
5	C(Montage)	-8.5e-16	2	-7.3e-14	1.0
	C(Time)	-1.1e-16	2	-9.2e-15	1.0
	C(Animal)	**0.62**	**1**	**10.6**	**<0.001**
	C(Montage):C(Time)	**0.12**	**4**	**5.3**	**<0.001**
	C(Montage):C(Animal)	1.0e-16	2	8.9e-15	1.0
	C(Time):C(Animal)	5.9-16	2	5.0e-14	1.0
	C(Montage):C(Time):C(Animal)	0.051	4	2.2	0.078
	Residual	0.56	95	NaN	
6	C(Montage)	1.9e-15	2	-4.2e-14	1.0
	C(Time)	-2.3e-16	2	-5.1e-15	1.0
	C(Animal)	**5.3**	**1**	**23.6**	**<0.001**
	C(Montage):C(Time)	**0.77**	**4**	**8.5**	**<0.001**
	C(Montage):C(Animal)	2.9e-16	2	6.4e-15	1.0
	C(Time):C(Animal)	4.9e-15	2	8.9e-14	1.0
	C(Montage):C(Time):C(Animal)	0.11	4	1.2	0.32
	Residual	2.1	95	NaN	

T-test independent sample, Bonferroni correction, comparing slope's coefficients

Compared conditions	*Mean (SD)*	*df*	*t-value*	*Adjusted p-value*
Before	1.5 (1.8)			
post-Anodal 2 mA	0.7 (1.5)	51	2.6	0.025

Supplementary Files

Supplementary File 1. Structural images showing the position of the tDCS electrodes on the monkey's head across sessions. Sagittal, coronal and transverse MRI sections, and corresponding skin reconstruction images showing the position of the prefrontal and occipital electrodes on the monkey's head for each MRI session (except for 4 sessions in which no anatomical scan was acquired). The two electrodes were accurately placed over the prefrontal cortex and the occipital cortex in a reproducible manner across sessions and between the two monkeys studied in each arousal state. In anesthesia experiments, the anodal electrode was placed over the dorsal prefrontal cortex, while the cathodal electrode was positioned over the parieto-occipital junction. In awake experiments, the prefrontal electrode was positioned over the dorsal prefrontal cortex/pre-motor cortex, while the occipital electrode was placed over the visual area 1. The position of the two electrodes differed slightly between the anesthetized and awake experiments due to different body positions (the prone position of the sedated monkeys prevented a more posterior position of the occipital electrode) and also due to the presence of a headpost on the head of the two monkeys in awake experiments (the monkeys we worked with in anesthesia experiments did not have an headpost).

Supplementary File 2. Complementary figures showing the analysis performed separately for the two monkeys reproducing the main findings. A) Slope analysis performed for both monkeys (Y. & J.) separately in the only awake conditions. **B)** Shannon entropy analysis performed for both monkeys (Y. & J.) separately in the only awake conditions. **C)** Slope analysis performed for both monkeys (Y. & J.) separately in the only anesthesia conditions. **D)** Shannon entropy analysis performed for both monkeys (Y. & J.) separately in the only anesthesia conditions.

Supplementary File 3. FC matrices changes and effects of tDCS stimulation on classical functional graph properties in awake dataset. A) Particular region-to-region functional links are depicted by their *p* value significance when comparing pairs of conditions. **B)** Modularity of average FC matrices show no difference between conditions, **C)** neither does it when computed for all the visited functional phase-coherence states (for every timepoint, for all subjects), nor efficiency measure or density.

Supplementary File 4. FC matrices changes and effects of tDCS stimulation on classical functional graph properties in anesthesia dataset. A) Particular region-to-region functional links are depicted by their *p* value significance when comparing pairs of conditions. Not a single functional connection was find to be statistically significant. **B)** Modularity of average FC matrices show no difference between conditions, **C)** neither does it when computed for all the visited functional phase-coherence states (for every timepoint, for all subjects), nor efficiency measure or density.